© 2019. Published by The Company of Biologists Ltd | Development (2019) 146, dev174375. doi:10.1242/dev.174375

RESEARCH ARTICLE

miR167 limits anther growth to potentiate anther dehiscence

Lanjie Zheng[1,2], Punita Nagpal[1], Gonzalo Villarino[3,*], Brendan Trinidad[1], Laurina Bird[1], Yubi Huang[2] and Jason W. Reed[1,4,‡]

ABSTRACT

In flowering plants, anther dehiscence and pollen release are essential for sexual reproduction. Anthers dehisce after cell wall degradation weakens stomium cell junctions in each anther locule, and desiccation creates mechanical forces that open the locules. Either effect or both together may break stomium cell junctions. The microRNA miR167 negatively regulates *ARF6* and *ARF8*, which encode auxin response transcription factors. *Arabidopsis mARF6* or *mARF8* plants with mutated miR167 target sites have defective anther dehiscence and ovule development. Null *mir167a* mutations recapitulated *mARF6* and *mARF8* anther and ovule phenotypes, indicating that *MIR167a* is the main miR167 precursor gene that delimits *ARF6* and *ARF8* expression in these organs. Anthers of *mir167a* or *mARF6/8* plants overexpressed genes encoding cell wall loosening functions associated with cell expansion, and grew larger than wild-type anthers did starting at flower stage 11. Experimental desiccation enabled dehiscence of miR167-deficient anthers, indicating competence to dehisce. Conversely, high humidity conditions delayed anther dehiscence in wild-type flowers. These results support a model in which miR167-mediated anther growth arrest permits anther dehiscence. Without miR167 regulation, excess anther growth delays dehiscence by prolonging desiccation.

KEY WORDS: Anther dehiscence, miR167, *mARF6*, *mARF8*, Ovule, *Arabidopsis thaliana*

INTRODUCTION

Release of pollen from anthers is essential for sexual reproduction of flowering plants. The diurnal and developmental timing of anther dehiscence affects the mode of pollination and the degree of selfing versus outcrossing. Timing of anther dehiscence is also important for pollination and seed production in breeding programs and agriculture. Anther dehiscence often occurs when flowers open at anthesis, at flower stage 13 in *Arabidopsis thaliana* (Smyth et al., 1990). Before anther dehiscence, cells in the septum between locules die and break down, lignin is deposited in cell walls surrounding the endothecium cell layer just beneath the epidermis, pectin in cell walls of the stomium breaks down and the anther desiccates. These processes lead to rupture of the stomium, anther opening and pollen release (Wilson et al., 2011; Nelson et al., 2012).

[1]Department of Biology, University of North Carolina at Chapel Hill, Chapel Hill, NC 27599-3280, USA. [2]College of Agronomy, Sichuan Agricultural University, Chengdu, Sichuan 611130, China. [3]Department of Plant and Microbial Biology, North Carolina State University, Raleigh, NC 27695, USA. [4]Laboratoire de Reproduction et Developpement des Plantes, Ecole Normale Superieure de Lyon, 69342 Lyon, France.
*Present address: Department of Biology, San Diego State University, San Diego, CA 92182, USA.

‡Author for correspondence (jreed@email.unc.edu)

L.Z., 0000-0001-8001-0695; G.V., 0000-0003-2832-6785; J.W.R., 0000-0001-7508-9714

Received 28 November 2018; Accepted 21 June 2019

In *Arabidopsis*, a network of hormone signaling pathways regulates the timing of flower maturation and anther dehiscence. Gibberellins and the redundantly acting auxin response transcription factors ARF6 and ARF8 are each required for production of jasmonate hormones in flowers at stages 11-12, shortly before flowers open (Nagpal et al., 2005; Cheng et al., 2009; Tabata et al., 2010; Reeves et al., 2012). Jasmonates, in turn, activate genes encoding the transcription factors MYB21 and MYB24, which then stimulate anther dehiscence (Mandaokar et al., 2006; Cheng et al., 2009; Reeves et al., 2012). In addition, MYB21 and MYB24 proteins can interact with MYC bHLH transcription factors, which mediate the jasmonate response, and with JAZ repressors of jasmonate signaling, suggesting that jasmonate may also regulate the transcriptional activation activity of MYB21 and MYB24 (Song et al., 2011; Qi et al., 2015; Huang et al., 2017). Anthers of mutants deficient in these components arrest at flower stage 12 just prior to anther dehiscence, with absent or delayed stomium rupture (Feys et al., 1994; Sanders et al., 2000; Ishiguro et al., 2001; Park et al., 2002; von Malek et al., 2002; Nagpal et al., 2005; Mandaokar et al., 2006; Reeves et al., 2012). In *Arabidopsis*, ARF6 and ARF8 are also required for female fertility, whereas jasmonate, MYB21 and MYB24 only regulate stamen and petal development. In tomato, ARF6 and ARF8 are similarly important for gynoecium, stamen and petal development (Liu et al., 2014), whereas jasmonates and SlMYB21 regulate gynoecium development but not stamen development (Li et al., 2004; Schubert et al., 2019). In developing *Arabidopsis* flowers, *ARF6* and *ARF8* are expressed in stamen filaments, where jasmonate is predominantly produced (Ishiguro et al., 2001; Wu et al., 2006). Jasmonates can move to other cells, and jasmonate response in the anther epidermis is sufficient for anther dehiscence (Jewell and Browse, 2016). After flowers open, jasmonate and MYB21 levels decrease through a negative feedback (Nagpal et al., 2005; Reeves et al., 2012).

Although *ARF6* and *ARF8* are required to initiate this pathway for jasmonate production and anther dehiscence, they also need to be inhibited for anthers to dehisce. Loss of negative regulation by the microRNA miR167 by mutation of the miR167 target site in either *ARF6* or *ARF8* causes both male and female sterility, due to ectopic expression of *ARF6* or *ARF8* in anthers and ovules (Wu et al., 2006). Stomium rupture does not occur in anthers of strong *mARF6* plants. Moreover, anthers of *mARF6* and *mARF8* plants are larger than anthers of wild-type, jasmonate-deficient or *myb21 myb24* double mutants. *mARF6* anthers have ectopic expression of *ARF6* in cells surrounding the anther vasculature, where miR167 is present in wild-type anthers, and this expanded expression domain likely underlies the anther phenotype (Válóczi et al., 2006; Wu et al., 2006; Rubio-Somoza and Weigel, 2013).

These studies have shown that anther dehiscence occurring at flower stage 13 requires correct spatial regulation of *ARF6* and *ARF8*. In addition, anthers of auxin receptor mutants with decreased auxin response, or of mutants with altered auxin transport, dehisced precociously, suggesting that auxin response normally inhibits

Development (2019) 146, dev174375. doi:10.1242/dev.174375

anther dehiscence at earlier developmental stages (Cecchetti et al., 2008, 2013, 2015). Excess auxin production in rice anthers also delays dehiscence (Song et al., 2018). The early dehiscence of *Arabidopsis* auxin pathway mutants was attributed to a combination of precocious lignification and jasmonate production in auxin-resistant mutant anthers (Cecchetti et al., 2013). The precocious anther dehiscence of these mutants contrasts with the delayed dehiscence of *arf6 arf8* double mutants, and suggests that distinct auxin responses may regulate anther dehiscence differently. In fact, auxin receptor mutants had decreased auxin response in the middle layer of the anther wall, whereas *ARF6* and *ARF8* are expressed in stamen filaments but not in cells that surround anther locules (Wu et al., 2006; Cecchetti et al., 2016). Thus, auxin response in different cells of the stamen may cause contrasting overall effects on anther dehiscence.

Here, we have engineered plants with mutations in the *MIR167a* gene encoding pre-miR167, and compared anther growth and morphology among wild-type, *mir167a* and *mARF6/8* plants. Analyses of gene expression in wild-type, *mARF6* and *mARF8* stamens suggest that miR167-mediated clearance of *ARF6* and *ARF8* from anthers limits expression of growth-promoting genes at flower stages 11-12, and thereby enables anther dehiscence at stage 13. Manipulations of hydration status suggest that changes in miR167 function do not affect competence to dehisce. Rather, anther size affects the duration of anther desiccation, which then determines the timing of dehiscence.

RESULTS

Mutations in *MIR167a* recapitulate *mARF6* and *mARF8* phenotypes

mARF6 and *mARF8* constructs have genomic *ARF6* or *ARF8* genes with mutations at the target site of miR167. Different transgenic plant lines carrying either of these constructs had a range of phenotypes, and were both male- and female-sterile (Wu et al., 2006). We screened additional transformants, and identified one *mARF6* and two *mARF8* lines that had delayed anther dehiscence (Fig. 1) and reduced fecundity, but that produced a small number of seeds after self-pollination of hemizygotes, or after outcrossing pollen from hemizygotes to a wild-type recipient. Homozygotes, obtained from self-pollinated hemizygotes, released a small amount of pollen only in quite old flowers, and were also entirely female-sterile due to defective ovule integument growth (Fig. 2). These lines segregated as single-locus lines in progeny of crosses. Stamens from *mARF6* and *mARF8* stage 11 flower buds had higher levels of *ARF6* or *ARF8* mRNA than did wild-type stamens (Fig. 1A). As these lines could be propagated, they allowed more extensive analyses of phenotypes than was achieved previously using T1 plants (Wu et al., 2006).

Four *MIR167* precursor genes encode miR167 in *Arabidopsis*. Analyses of promoter:GFP:GUS fusion plants have revealed that stamens express both *MIR167a* and *MIR167c* (Wu et al., 2006; Rubio-Somoza and Weigel, 2013). $P_{MIR167a}$*:GUS* anthers had X-Gluc staining in the vicinity of the anther vasculature at flower stages 10-12, and then throughout the anther starting at late stage 12, approximately one flower before the first open flower (Fig. 3A-E, Fig. S1A). In addition to the previously reported expression in stage 13 stamen filaments, $P_{MIR167c}$*:GUS* anthers had X-Gluc staining throughout young anthers until early stage 11, approximately six flowers before the first fully open flower, after which anther staining disappeared (Fig. S1G).

Strong $P_{MIR167a}$*:GUS* expression in stage 11 and 12 anthers suggested that the *MIR167a* precursor gene might produce the miR167 that represses *ARF6* and *ARF8* in anthers. We generated plants with mutations in *MIR167a* using CRISPR/Cas9-based genome engineering to target a site within the 21 nt miR167 sequence (Fig. 1K). Among the T2 plants derived from self-fertilization of T1 transformants that had carried the genome engineering construct, several had flower phenotypes resembling those of *mARF6* or *mARF8* plants (Fig. 1G). DNA sequencing of the *MIR167a* gene from five of these revealed that four plants were transheterozygous for two different *mir167a* alleles, and one plant was homozygous for a single allele (Fig. 1K). We recovered seed from two of these plants and identified progeny that were homozygous for either *mir167a-1* (29 bp deletion including 14 bases of the 5′ end of mature miR167), *mir167a-2* (1 bp insertion of a G after position 15 of miR167) or *mir167a-8* (14 bp deletion including 7 bases at the 3′ end of mature miR167). qRT-PCR assays indicated that both the *mir167a-1* and *mir167a-2* mutant stamens had very low levels of mature miR167, although *ARF6* and *ARF8* transcript levels appeared normal, possibly reflecting high baseline expression in wild-type filaments (Fig. 1B).

mir167a mutants had delayed anther dehiscence (Fig. 1G) and produced no or very few seeds, either after manual self-pollination or in crosses with wild-type plants as either the male or female parent. Similarly to *mARF6* and *mARF8*, many of the seeds that *mir167a* plants produced were inviable. *mARF6-A/–* hemizygotes, *mARF8-3/–* hemizygotes and *mir167a* mutant plants had a mixture of ovules with short integuments similar to those of *mARF6* and *mARF8* homozygotes, and ovules with normal integuments (Fig. 2B-F), which may have given rise to the viable seed. F1 heterozygous *mir167a-1/+* and *mir167a-2/+* plants were fully fertile, and produced F2 progeny that segregated into roughly 25% presumed *mir167a* homozygotes with largely sterile flowers, consistent with a single locus being responsible for the phenotype (wt:mutant numbers for *mir167a-1*, 174:45 and for *mir167a-2*, 118:41; data pooled from several crosses).

The very similar phenotypes of *mir167a*, *mARF6* and *mARF8* plants indicate that *MIR167a* is the major miR167 precursor gene regulating *ARF6* and *ARF8* in flowers. Although *mARF6* and *mARF8* plants were difficult to propagate because of poor seed viability, the stronger phenotypes of *mARF6* and *mARF8* homozygotes compared with *mir167a* mutants gave more definitive results in some experiments. Moreover, partially dominant *mARF6* or *mARF8* lines were convenient for experiments with reporter genes using F1 plants.

mir167 limits anther growth after flower stage 11

Wild-type anthers had a projected area of ∼0.15 mm^2 viewed from the adaxial side at late flower stage 11 or early stage 12 (gynoecium length 1.3-1.5 mm, approximately 4 flowers before opening), and grew slightly up through stage 12 just before flowers opened, when gynoecia were ∼2 mm long (Fig. 4A,B). During stage 12, stamen filaments typically grow much faster, roughly doubling in length (Smyth et al., 1990; Reeves et al., 2012). At stage 13 when flowers opened, wild-type anthers began to shrink, and they dehisced to release pollen (Fig. 4A-C).

In *mARF6* and *mARF8* flowers, petal and stamen filament growth proceeded normally through flower maturation and opening (Fig. S2A,B), but anthers grew too large at flower stages 11-12 (Smyth et al., 1990). At stage 11, approximately 5-6 flowers before the first open flower, *mARF6* and *mARF8* anthers developed a broader cap of cells at the apical end than did wild-type anthers, and they became measurably larger than wild-type anthers starting at approximately 4 flowers before the first open flower, when wild-type anther growth slowed (Fig. 4A,B, Fig. S3A,B,C).

Development (2019) 146, dev174375. doi:10.1242/dev.174375

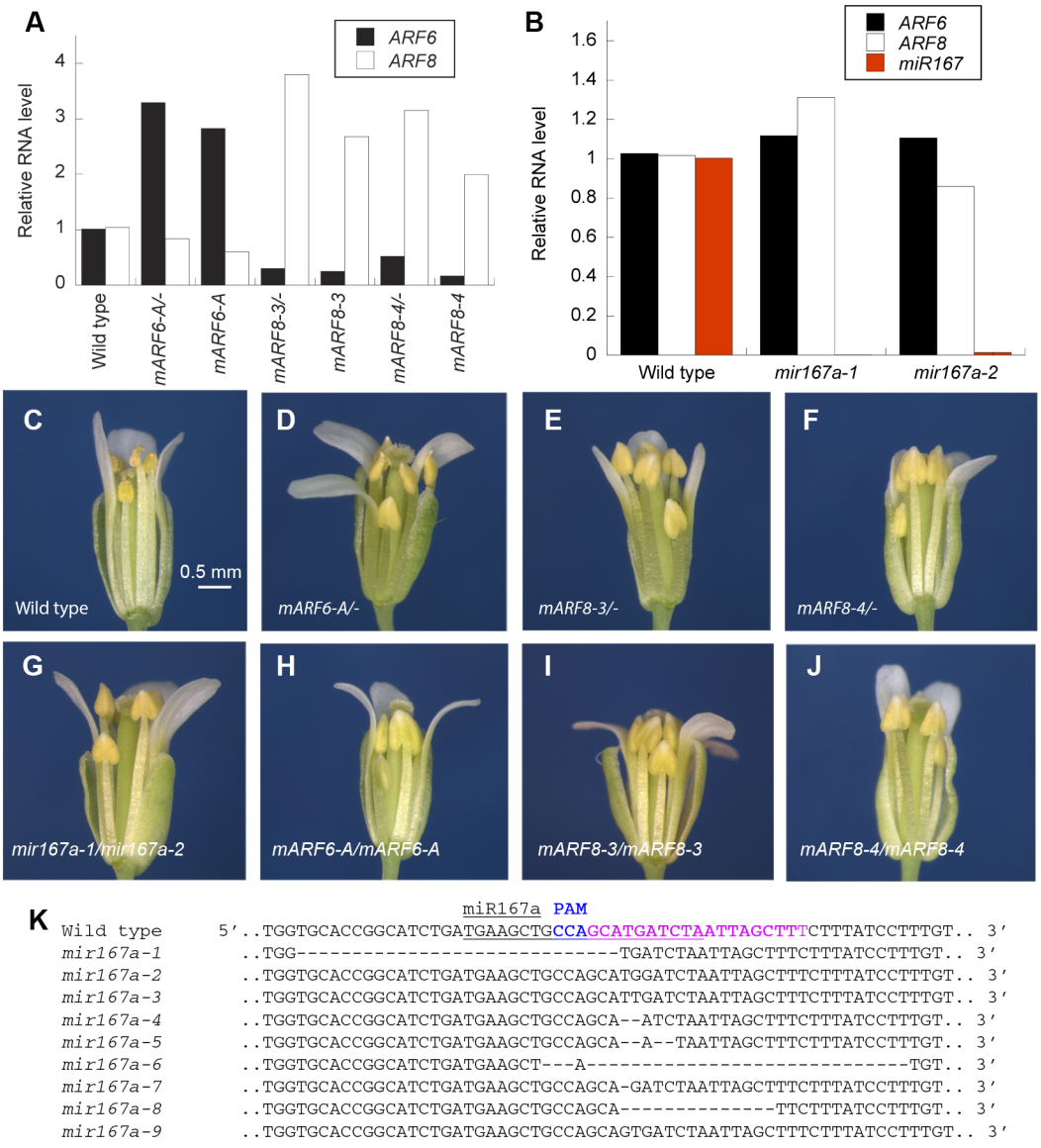

Fig. 1. Genotypes with disrupted mir167a action. (A) qRT-PCR of *ARF6* and *ARF8* levels in flower stage 11 stamens of hemizygous and homozygous *mARF6* and *mARF8* lines. A partial replicate experiment lacking *mARF6* samples gave similar results. (B) qRT-PCR of miR167 in wild-type and *mir167a* stage 12-13 pooled stamens. A replicate experiment gave similar results. In A and B, RNA levels were normalized to *UBQ* levels and to the wild-type mean. (C-J) Photographs of stage 13 flowers of indicated genotypes. (K) Sequenced *miR167a* mutations identified by sgRNA/Cas9-mediated targeted mutagenesis. On the wild-type sequence, underlined characters indicate the mature miR167a sequence, blue characters indicate the complementary sequence to the protospacer adjacent motif (PAM) and purple characters indicate the complementary sequence of the designed sgRNA.

Hemizygous *mARF6/–* and *mARF8/–* anthers grew to be up to 25% larger in projected area than did wild-type anthers, shrank somewhat starting at the time of flower opening and dehisced 2 to 3 flowers later than did wild-type anthers, although they generally opened less widely and released less pollen than did wild-type anthers (Fig. 4A, C). Homozygous *mARF6* and *mARF8* anthers also grew larger than did wild-type anthers, shrank less after flower opening and usually failed to dehisce (Fig. 4A-C, Fig. S3A-C). *mir167a* mutant plants had enlarged and indehiscent anthers similar to those of *mARF6* and *mARF8* plants (Fig. 4A,G, Fig. S3A). Anther dehiscence in *mir167a* mutants occurred later than it did in *mARF6/–* or *mARF8/–* hemizygotes, but earlier than in *mARF6* or *mARF8* homozygotes (Fig. 4C, Fig. S2C). As a result of the excess growth of locules and of cells at the tip, the anthers of *mir167a*, *mARF6* and *mARF8* plants developed a spade-shaped appearance.

Epidermal cells of *mir167a*, *mARF6*, and *mARF8* anthers were visibly larger than those in wild-type anthers, especially in the area close to the junction with the filament (Fig. 4D-F). In transverse cross-sections, *mARF8* and *mir167a* anthers from the first open flower (stage 13) had similar cellular organization to wild-type anthers, but had larger connective, epidermis and endothecium cells, and were larger than wild-type anthers across the lateral and adaxial-abaxial axes, similarly to *mARF6* anthers characterized previously (Fig. 5A-D) (Wu et al., 2006). In some *mir167a-1* and *mARF8-3* anther locules, the septum had degraded and the stomium was broken, although the anther locules had not opened to release pollen as they did in wild-type anthers (Fig. 5B,D). In other mutant anthers, the septum was incompletely degraded and/or the stomium was still connected (Fig. 5C). Often, different sections from the same anther revealed different degrees of septum or stomium

Development (2019) 146, dev174375. doi:10.1242/dev.174375

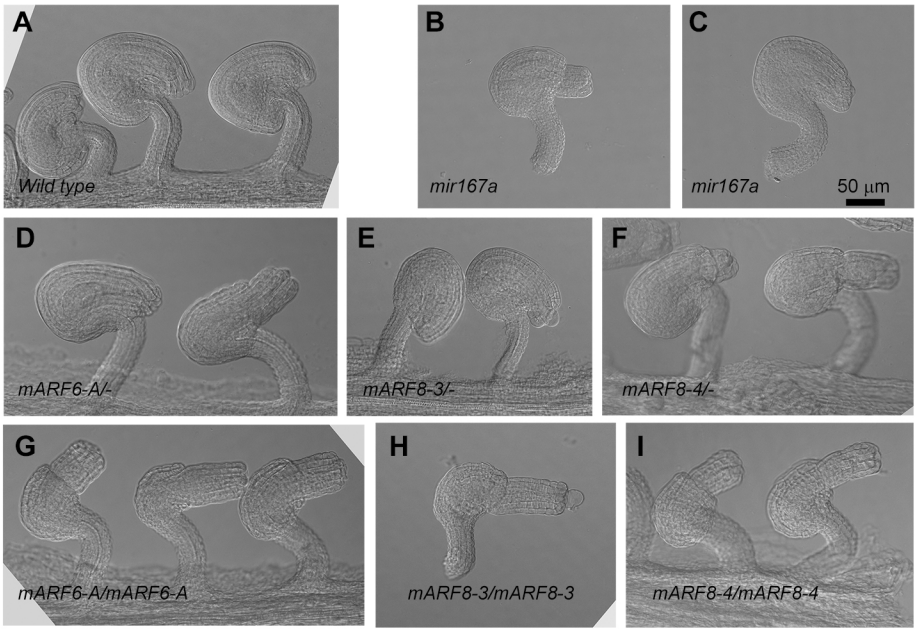

Fig. 2. Ovule phenotypes of mature stage 13 flowers. (A) Wild type. (B,C) *mir167a-1*/*mir167a-2*. (D,E,F) Hemizygous *mARF6-A*/–, *mARF8-3*/–, and *mARF8-4*/– ovules. (G,H,I) Homozygous *mARF6-A*, *mARF8-3* and *mARF8-4*. Individual gynoecia of *mir167a*, *mARF6*/– and *mARF8*/– genotypes had a mixture of ovules with normal appearance and ovules with outer integuments that failed to extend around the ends of the inner integuments. Scale bar: 50 µm.

breakage, implying that only part of the septum and stomium had broken. Similarly, in images taken by environmental scanning electron microscopy (eSEM) (Fig. 5E-L), stage 13 and 14 *mARF8* anthers sometimes appeared partially open, with a slit along part of the dehiscence zone (Fig. 5G,K). In addition, some *mARF8* anthers had pollen grains that had germinated within the anther locule (Fig. 5C,D, arrows).

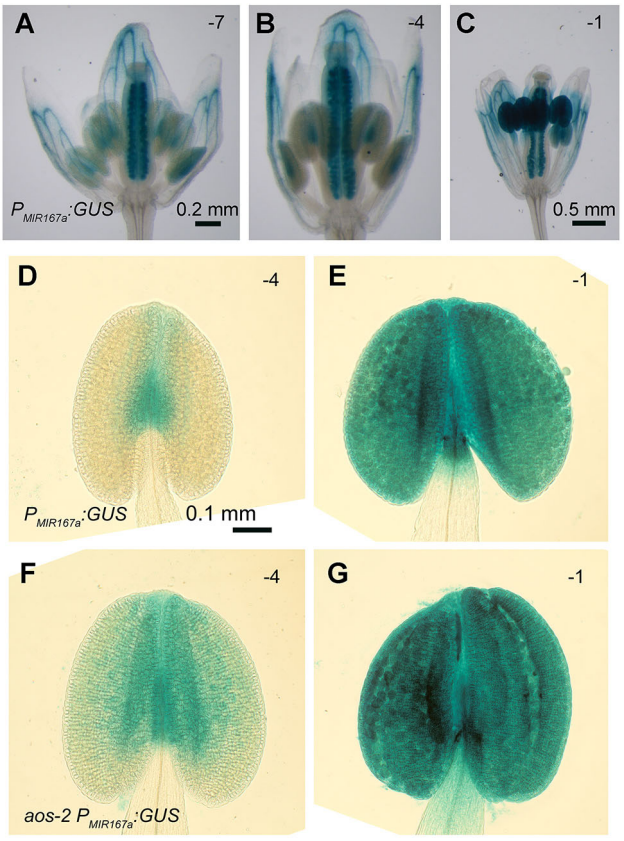

Fig. 3. $P_{MIR167A}$:*GUS* X-Gluc staining in flowers and anthers. (A-C) Images of X-Gluc staining in flowers at indicated stages. –7, seventh bud before first open flower; –4, fourth bud before first open flower; –1 largest closed bud. (D-G) X-Gluc-stained wild-type (D,E) and *aos-2* (F,G) anthers at indicated flower bud stages. Scale bars: 0.2 mm (A,B), 0.5 mm (C), 0.1 mm (D-G).

Pollen from *mir167a*, *mARF6* or *mARF8* plants had apparently normal exterior morphology by eSEM (Fig. S4A-D). As assessed by fluorescein diacetate staining, pollen from the first open flower of *mir167a*, *mARF6* or *mARF8* plants (obtained by cutting open the anthers) had similar viability to pollen from wild-type flowers, whereas pollen from the fifth open flower was somewhat less viable than pollen from the fifth open wild-type flower (Fig. S4E). Moreover, *mir167a* and *mARF8* pollen germinated *in vitro* at a ∼20% lower rate than did wild-type pollen (Fig. S4F). The decreased pollen performance of these genotypes may contribute to their decreased pollination efficiency.

Consistent with their increased and persistent growth, *mARF6*/– and *mARF8*/– anthers had increased signal of a phloem unloading tracer, P_{SUC2}:*YPET*, which is expressed in phloem companion cells of source tissues and delivered to sink tissues such as anthers (Truernit and Sauer, 1995; Imlau et al., 1999; Stadler et al., 2005a,b). In wild-type anthers, P_{SUC2}:*YPET* fluorescence appeared in cells surrounding the vasculature in the center of the anther up until the third open flower, but then decreased starting after flower +3. (Fig. 6A,B,F). In *mARF6*/– and *mARF8*/– anthers, P_{SUC2}:*YPET* signal in cells surrounding the anther vasculature continued up to approximately flower +6 (Fig. 6C-E). In addition, the phloem domain was longer in *mARF6*/– and *mARF8*/– anthers than in wild-type anthers starting at flower −4 and continuing up until flower +6 (Fig. 6F). Thus, it appears that phloem content was delivered into *mARF6*/– and *mARF8*/– anthers over a larger area and until a later stage than occurs in the wild type. This phenotype may arise simply because the *mARF* anthers grow larger, but could also contribute to their increased growth.

In wild-type, *mARF6* and *mARF8* anthers, phloroglucinol stained a stripe of lignin near the future dehiscence zone on each half of the anther, similar in extent in each genotype (Fig. 6I-K) (Mizuno et al., 2007; Cecchetti et al., 2016). Appearance of the lignification zone in *mARF6* and *mARF8* anthers suggests that their delayed dehiscence does not arise from a failure of lignin deposition as in *myb26* mutants (Yang et al., 2007). In addition,

Development (2019) 146, dev174375. doi:10.1242/dev.174375

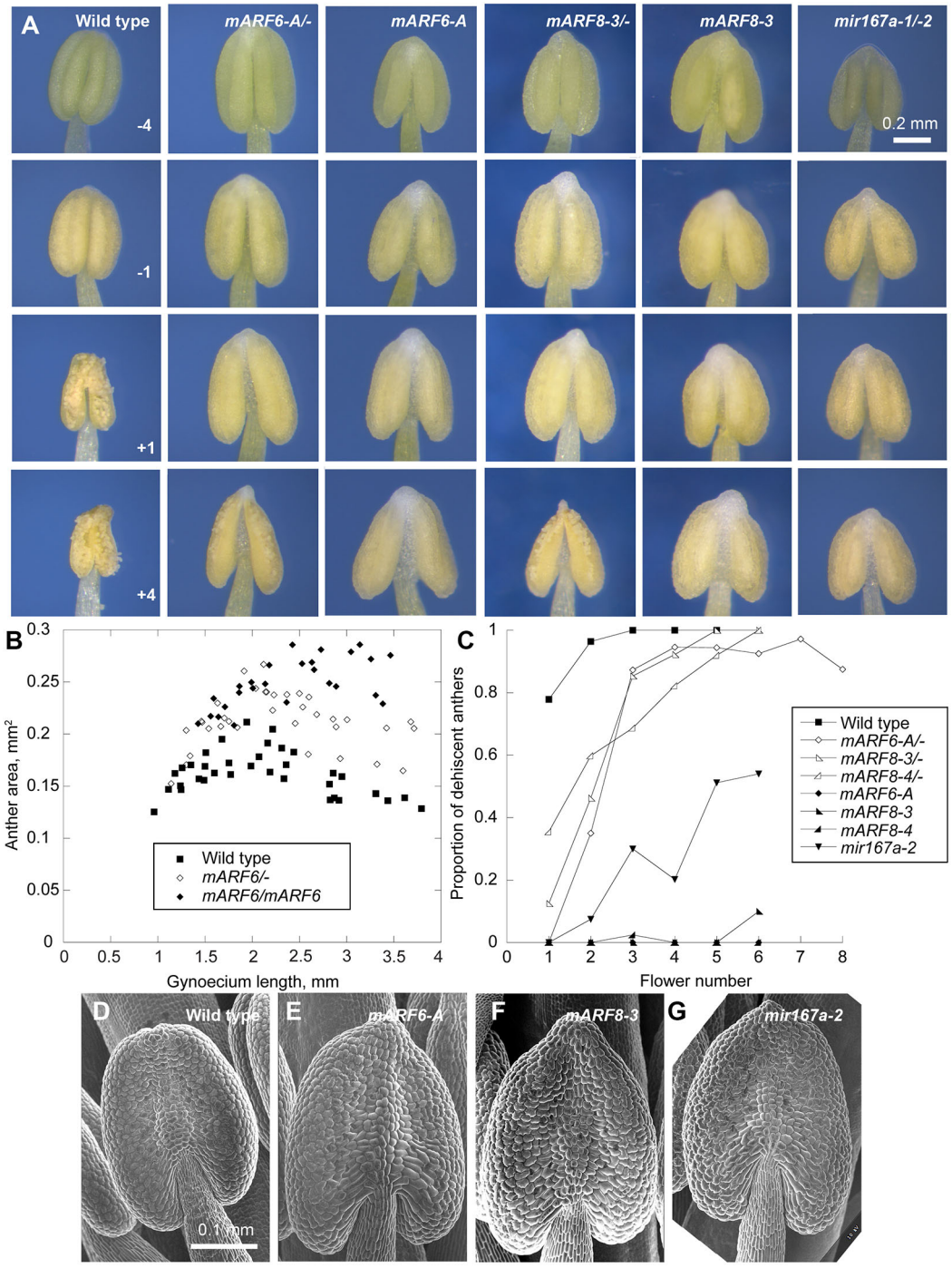

Fig. 4. Anther phenotypes of plants with disrupted miR167 action. (A) Photographs of anthers at indicated stages. −4, fourth bud before first open flower; −1, largest closed bud; +1, first open flower; +4, fourth open flower. Fig. S3 shows images of anthers in additional genotypes and stages. (B) Anther projected area measurements for wild-type, *mARF6-A*/− hemizogous and *mARF6-A* homozygous plants over a developmental series. Gynoecium length was used as an internal reference to stage the flowers. Fig. S3 shows similar data for additional genotypes. (C) Timing of anther dehiscence. Shown is the proportion of flowers at each consecutive open flower position with at least half of the anthers releasing pollen. +1, first open flower. *n*=3-14 flowers for each point, except *n*=2 for *mARF8-3* homozygote flower at +6. Older flowers shed their stamens and other organs, precluding analyses of higher numbers at late stages. Fig. S2C shows additional data for another experiment including both *mir167a-1* and *mir167a-2* mutants. (D-G) SEM of abaxial anther surface of indicated genotypes. Gynoecia were 0.93-0.98 mm long, corresponding to late stage 11/early stage 12 flowers. Scale bars: 0.2 mm (A), 0.1 mm (D-G).

differentiated stomata were visible on the abaxial side of *mARF6*, *mARF8* and *mir167a* anthers, as in wild-type anthers (Fig. 4D-G, Fig. 6G,H). Thus, *mARF6* and *mARF8* anthers differ from wild-type anthers mainly in size rather than in other anatomical features that can affect dehiscence.

mARF8 stamens overexpress genes that may regulate growth

We assayed global gene expression patterns by RNA-Seq in wild-type and *mARF8* stamens from flower stage 11, when the excess growth begins. The *mARF8* samples came from both stable *mARF8*

Development (2019) 146, dev174375. doi:10.1242/dev.174375

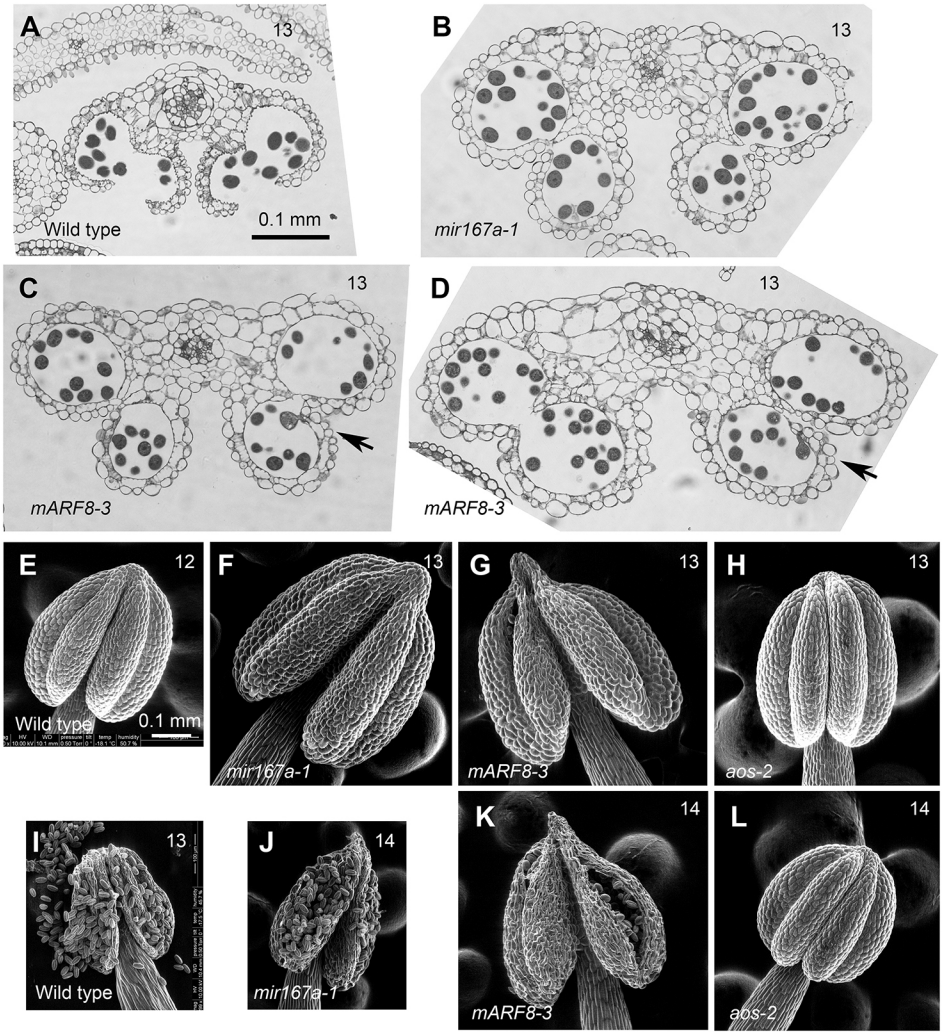

Fig. 5. Microscopy of *mARF* and *mir167a* anthers. (A-D) Bright-field images of transverse sections of stage 13 (first open flower) anthers of indicated genotypes. Arrows in C and D indicate germinated pollen grains. (E-L) eSEM images of the adaxial side of anthers of indicated genotypes at indicated flower stages. Scale bars: 0.1 mm (A-L).

lines characterized here, and from a pooled sample from T1 *mARF8* plants that were not recovered as stable lines (Table S1). In addition, we included samples from stamens of P_{RPS5a}>*MIR167a* plants overexpressing *MIR167a*. These plants resemble *arf6 arf8* double mutant plants (Reed et al., 2018), and reveal effects of loss of the redundantly acting ARF6 and ARF8.

Using DESeq2 software, we identified genes whose expression was statistically significantly different between wild-type and P_{RPS5a}>*MIR167a* stamens, or between wild-type and *mARF8* stamens, and that also had at least two-fold difference in expression levels (Fig. 7A, Tables S2-S4). In P_{RPS5a}>*MIR167a* stamens, more genes were underexpressed (969) than were overexpressed (292) (Table S2), consistent with previous microarray results of *arf6 arf8* whole flowers (Nagpal et al., 2005; Reeves et al., 2012), and with the finding that ARF6 and ARF8 activate gene expression (Ulmasov et al., 1999). Of 624 genes previously found to be underexpressed in microarray analyses of *arf6-2 arf8-3* stage 12 flower buds (Reeves et al., 2012), 177 (28%) were also underexpressed in the stage 11 P_{RPS5a}>*MIR167a* stamens studied here (Table S2). Considering that the previous experiment was based on whole flowers and at a slightly later stage than stamens of the current experiment, the overlap suggests good concordance of the datasets. Genes overexpressed in the ARF-deficient flowers or stamens in both datasets had less overlap (29 in common of 312 genes from the Reeves et al., 2012 dataset), suggesting that more of the overexpressed genes may be affected indirectly or in other organs.

mARF8 stamens overexpressed 1105 genes, 102 of which were underexpressed in P_{RPS5a}>*MIR167a* stamens (Tables S3 and S4). *mARF8* stamens underexpressed 1686 genes, suggesting either that ectopic ARF8 also represses genes directly, or that many of the underexpressed genes are affected secondarily. qRT-PCR assays confirmed that *LOX2/At3g45140*, *SAUR42/At2g28085*, *At5g50335*, *XTH19/At4g30290* and *AXR2/IAA7/At3g23050* were each overexpressed in *mir167a*, hemizygous or homozygous *mARF6* and/or *mARF8* stamens at flower stage 11 (Fig. 7B,C, Fig. S5). In addition, *MYB26/At3g13890* was overexpressed in *mARF6* and *mARF8* stamens but not in *mir167a* stamens, although the expression level of *MYB26* in our experiment was generally very low and the results may therefore be sensitive to small differences in sample staging. In contrast, *EXPA8/At2g40610* was not overexpressed in the tested genotypes in most experiments. However, as described below, a *GUS* fusion to the promoter of *EXPA8/At2g40610* did have an expanded expression domain in *mARF6/−* anthers.

We surveyed groups of genes with different expression characteristics for enrichment of gene ontology (GO) categories, protein domains or Kyoto Encyclpedia of Genes and Genomes (KEGG) pathways (Tables S5-S10). The 102 genes that were underexpressed in P_{RPS5a}>*MIR167a* but overexpressed in *mARF8* stamens were enriched for the GO categories response to jasmonate

Development (2019) 146, dev174375. doi:10.1242/dev.174375

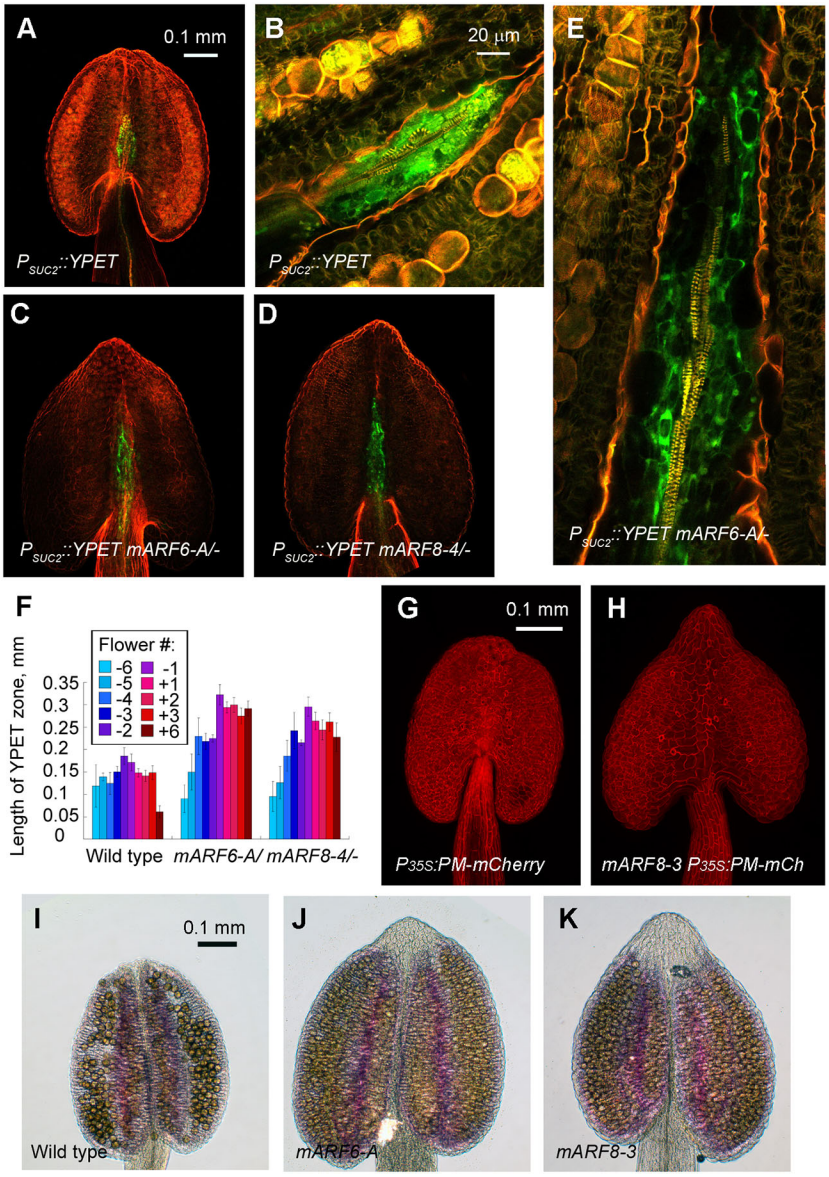

Fig. 6. Phenotypes of *mARF6* and *mARF8* anthers. (A-E) Extent of P_{SUC2}*:YPET* fluorescence in wild-type, *mARF6-A*/–, and *mARF8-4*/– stage 13 anthers. The image in E is a composite obtained by stitching together multiple images of different portions of the specimen. (F) Measurements of length of expression domain in wild-type and *mARF* anthers from indicated flowers. *n*=4-11 anther images per data point. Statistical results are not shown for clarity, but indicated means distinguishable from wild type for *mARF6*/– and *mARF8*/– at flower positions –4, –3, –2 (*mARF8-4*/– only), –1, +1, +2, +3, and +6 by Tukey's HSD test. (G,H) Confocal *z*-stack projections of abaxial sides of wild-type (G) and *mARF8-3* (H) anthers expressing the P_{35S}*:PM-mCherry* fluorescent marker. (I-K) Phloroglucinol staining of stage 13 anthers. Scale bars: 0.1 mm (for A,C,D,G-K); 20 µm (B,E).

(including jasmonate biosynthesis genes) and cell wall loosening (Table S6). Some of these genes may be direct ARF6 and ARF8 targets. In fact, 20 of these genes were designated as ARF6 targets in seedlings based on expression and ChIP-Seq data (Oh et al., 2014) (Table S6). *arf6 arf8* flowers underproduce jasmonates (Nagpal et al., 2005; Tabata et al., 2010; Reeves et al., 2012), and these results suggest that conversely, *mARF8* stamens may produce excess jasmonate. Cell wall loosening functions that may contribute to excess growth in *mARF8* anthers were represented by expansin genes (Cosgrove, 2016). Enriched protein domains included both expansins and a family of DUF642 proteins that are secreted to the apoplast and may be involved in pectin metabolism (Zúñiga-Sánchez et al., 2014; Salazar-Iribe et al., 2016).

The full set of 1105 genes that were overexpressed in *mARF8* stamens were similarly enriched for jasmonate pathway and cell wall loosening functions, and for fatty acid biosynthesis proteins and pathway, and the KEGG pathway term phenylpropanoid biosynthesis (Table S5). Overexpression of *MYB26/At3g13890* in *mARF8* stamens may contribute to the increased phenylpropanoid pathway gene expression (Table S5, Fig. 7B, Fig. S5). The transcription factor MYB26 activates the lignin biosynthesis pathway required to make the lignification zone in anthers (Yang et al., 2007). The jasmonate pathway is normally expressed at stages 11-12, but is then switched off in mature open flowers (Nagpal et al., 2005; Reeves et al., 2012). Overexpression of many of these genes in *mARF8* anthers may reflect persistent growth or delayed desiccation.

Enriched GO terms among genes that were underexpressed in both P_{RPS5a}*>MIR167a* and *mARF8* stamens included pollen tube growth and cation transport (Table S9). Enriched protein domains included pectin esterase inhibitors, RALF (rapid alkalinization factor) peptides, H^+/K^+ exchange transporters, and universal stress protein A domain (UspA) kinases (Kerk et al., 2003; Sze et al., 2004; Murphy and De Smet, 2014). Many of these are expressed in mature pollen or growing pollen tubes (Honys and Twell, 2004; Verelst et al., 2007a; Wang et al., 2008; Ge et al., 2017; Mecchia et al., 2017). In fact, 200 of the 411 genes that were underexpressed in both P_{RPS5a}*>MIR167a* and *mARF8* stamens were induced in tricellular and mature pollen (Honys and Twell, 2004; Verelst et al., 2007a) (Table S4). As that study used a microarray that has spots for approximately two-thirds of *Arabidopsis* genes, it seems likely

Development (2019) 146, dev174375. doi:10.1242/dev.174375

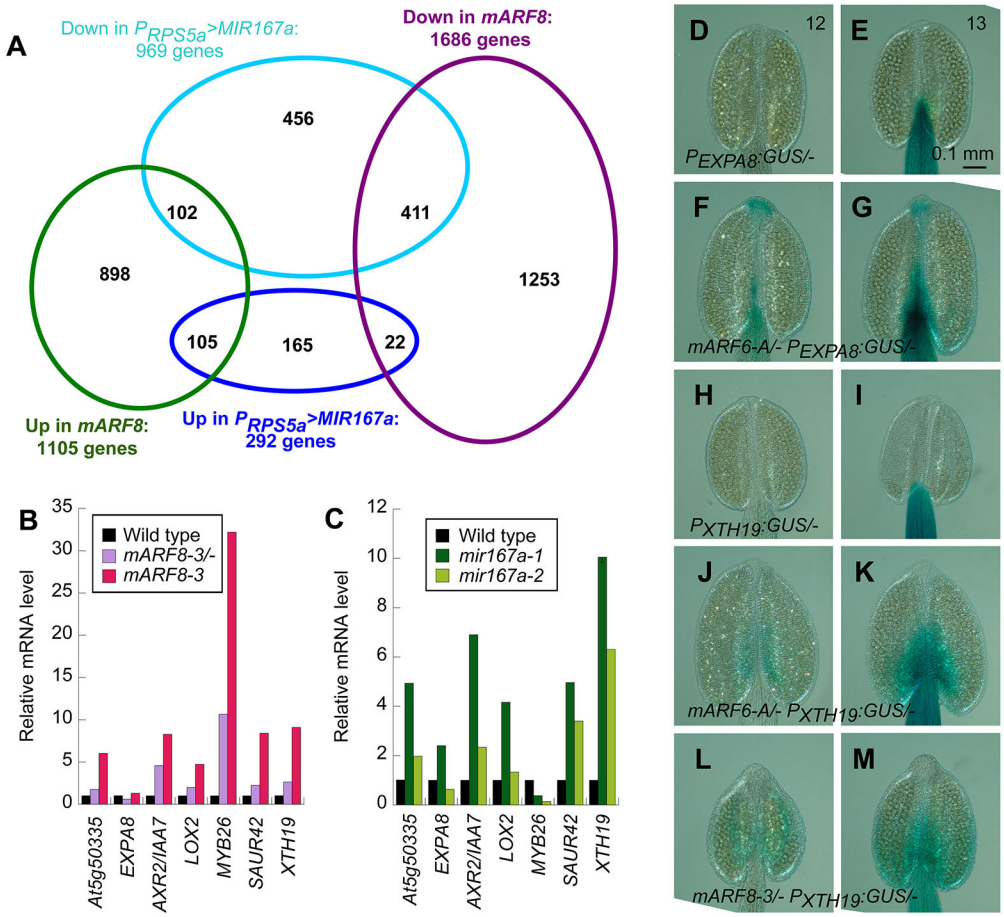

Fig. 7. Genes differentially expressed between wild-type and *mARF6* or *mARF8* stamens. (A) Venn diagram summarizing numbers of genes differentially expressed between wild-type and *mARF8* stage 11 stamens. (B,C) qRT-PCR of mRNA levels in stage 11 stamens of the indicated genotypes, for selected genes that were overexpressed in *mARF8* stamens in the RNA-Seq dataset. Fig. S5 shows a similar experiment with additional *mARF* genotypes. (D-M) X-Gluc staining of reporters P_{EXPA8}:*GUS* (D-G) and P_{XTH19}:*GUS* (H-M) in anthers of indicated genotypes at flower stages 12 and 13. Scale bar: 0.1 mm (D-M).

that a majority of the genes underexpressed in both P_{RPS5a}>*MIR167a* and *mARF8* are normally expressed in mature pollen. *mARF8* stamens underexpressed *AGL65*, *AGL66* and *AGL104*, which encode MADS-domain transcription factors that are required for late stages of pollen maturation (Verelst et al., 2007b). Their underexpression in P_{RPS5a}>*MIR167a* and *mARF8* stage 11 stamens suggests that pollen maturation or desiccation might be delayed in these stamens, and may have contributed to decreased *mARF8* pollination efficiency.

Expanded gene expression domain in *mARF6* and *mARF8* anthers

Both *EXPA8/At2g40610*, encoding an expansin protein, and *XTH19/At4g30290*, encoding a xyloglucan transglycosidase/hydrolase, were overexpressed in *mARF8* stamens based on our RNA-Seq data, and their products may contribute to cell wall loosening and growth. *EXPA8/At2g40610* is auxin regulated and considered to be a direct target of ARF6 in seedlings (Oh et al., 2014). We assessed expression of available P_{EXPA8}:*GUS* and P_{XTH19}:*GUS* fusions to the promoters of these two genes (Bassel et al., 2014) in F1 plants. Both had expanded expression domains in hemizygous *mARF6/–* or *mARF8/–* anthers. Wild-type P_{EXPA8}:*GUS* plants had X-Gluc staining in stamen filaments starting at stage 13, but did not have appreciable staining in anthers (Fig. 7D,E). In *mARF6/–* plants, staining appeared in anthers at stage 12 and persisted at stage 13 (Fig. 7F,G). The staining in *mARF6/–* anthers was confined to the central zone surrounding the vasculature and extended to the swollen tips of *mARF6/–* anthers. In wild-type P_{XTH19}:*GUS* stamens, X-Gluc staining was first visible in filaments starting at stage 12, and became stronger at stage 13; but was not detectable in anthers (Fig. 7H,I). In both *mARF6/–* and *mARF8/–* hemizygotes, staining was present in stage 12 and stage 13 anthers, with the strongest signal in cells surrounding the vasculature at the base of the anther (Fig. 7J-M).

Expanded expression domains of these reporters in *mARF6/–* or *mARF8/–* anthers could arise from excess ARF6 or ARF8 activity in the cells surrounding the anther vasculature. Visible X-Gluc stain in each case appeared at stage 12, which is slightly later than the action of miR167 at stage 11.

DR5:GUS expression persists in *mARF6* and *mARF8* anthers after flowers open

The auxin response reporter gene *DR5:GUS* is normally expressed in wild-type anthers primarily in the middle layer interior to the endothecium at flower stage 10, and is then turned off at approximately stage 11 (Aloni et al., 2006; Cecchetti et al., 2016) (Fig. S6A,H-J). In contrast, in anthers of *mARF6* and *mARF8* plants *DR5:GUS* expression persisted until well after flowers opened (Fig. S6B-E,K-M). Expression was generally stronger and persisted for longer in homozygotes than in hemizygotes. This expression was not confined to perivascular cells where ectopic *ARF6* and *ARF8* are likely to be present, but appeared to be in cells around the anther locules, suggesting indirect regulation.

To test whether ARF6 and ARF8 are necessary for *DR5:GUS* expression at earlier stages, we transformed the *DR5:GUS* line with a P_{35S}:*MIR167a* transgene that causes overproduction of miR167 and therefore reduces *ARF6* and *ARF8* mRNA levels (Wu et al., 2006). Inflorescences of several transformants with phenotypes

Development (2019) 146, dev174375. doi:10.1242/dev.174375

resembling those of strong *arf6 arf8* plants were stained with X-Gluc. In each case, significant staining was present in anthers (Fig. S6F,G). These results indicate that ARF6 and ARF8 are not required for *DR5:GUS* expression in anthers.

Desiccation promotes anther dehiscence in the absence of miR167 regulation

When *mARF6*, *mARF8* and *mir167a* inflorescences were cut off the plant and allowed to desiccate, anthers of stage 13 flowers released pollen (Fig. 8A,B), in contrast to the indehiscent anthers of well-watered intact plants. This observation suggests that delayed or failed dehiscence of *mARF6*, *mARF8* and *mir167a* anthers might be a consequence of excess water content arising from persistent growth. To test this model, we excised indehiscent stamens from flowers at defined developmental stages, and incubated them in air without a water source. Wild-type anthers from stage 12 unopened flowers usually dehisced to release pollen, whereas anthers from stage 11 flowers generally did not dehisce (Fig. 8D,E). *mARF6*, *mARF8* and *mir167a* anthers also dehisced in these experiments if they came from flower stage 12 or later (Fig. 8D,E, Fig. S7A,B). Dehiscence after stamen excision usually occurred within 2 h. Pollen obtained from desiccated homozygous *mARF6-A* anthers was used successfully to fertilize wild-type gynoecia, indicating that at least a portion of it was viable. These results indicate that miR167 action accelerates dehiscence but is not required to establish competence to dehisce in anthers of stage 12 flowers.

To create conditions of high humidity, we placed cut inflorescences in agar on vertically oriented Petri plates sealed against water loss. Many water droplets condensed on the plate lid, indicating that humidity in the air space was close to saturation. Inflorescences grew for at least 2 days under these conditions, and flower buds opened. However, even wild-type anthers did not dehisce while kept in high humidity (Fig. 8C). Once inflorescences or excised anthers were removed to a dry environment, the anthers shrank and dehisced (Fig. 8F-J). Similarly, *mir167a* stamens subjected to the vacuum used for eSEM imaging without mounting on a cooled (−20°C) stage dehisced within minutes (Fig. 8K,L). We compared the speed of dehiscence of anthers of matched developmental stage upon a shift from high to low humidity, after excising stamens from stage 13 flowers that had opened under high humidity without anther dehiscence. Wild-type anthers generally dehisced within 10 min of the shift, whereas anthers from *mir167a*, *mARF6* or *mARF8* plants

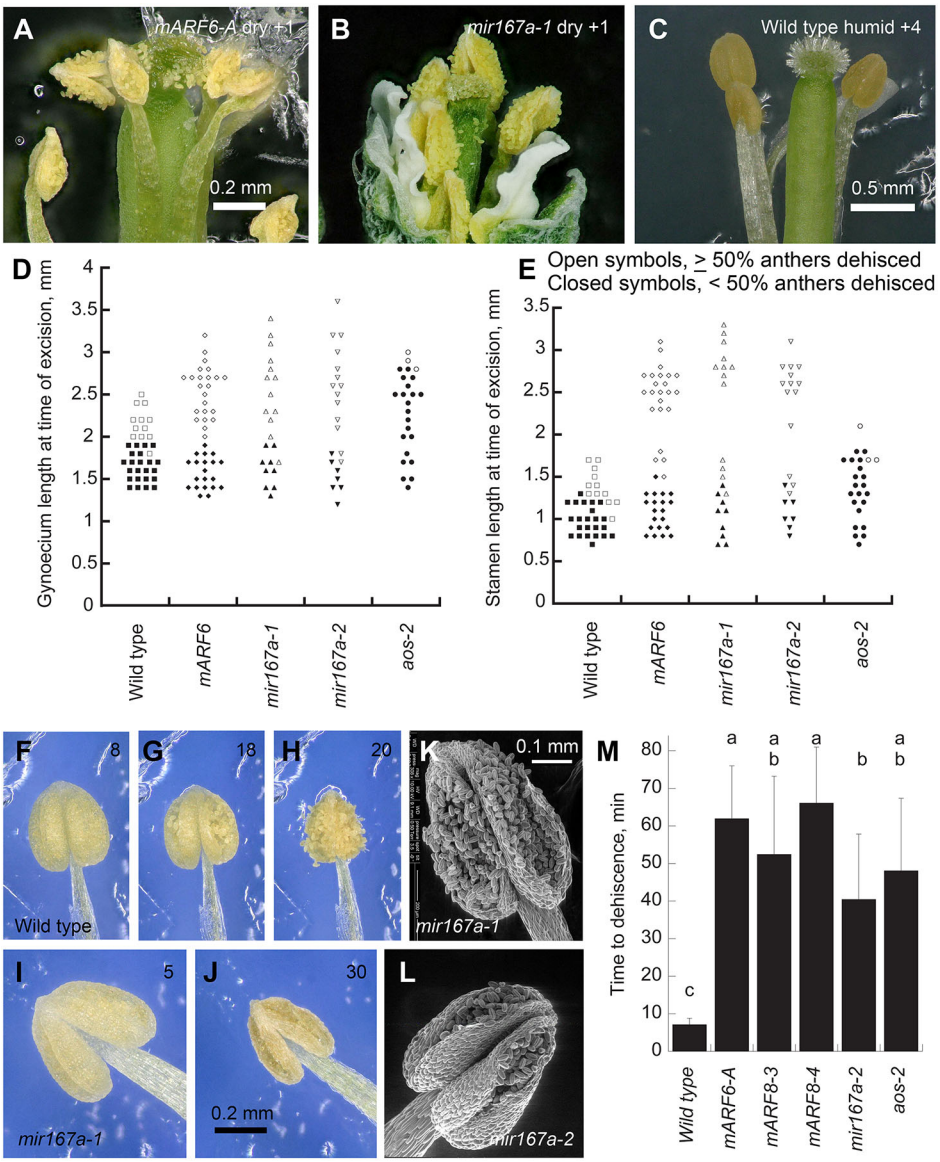

Fig. 8. Manipulation of anther desiccation rate. (A,B) Desiccated *mARF6-A* (A) and *mir167a* (B) stage 13 flowers (+1, first open flower), showing dehisced anthers releasing pollen. (C) Anthers of flower +4 (stage 14) from a wild-type inflorescence kept in high humidity conditions. (D,E) Summary of excised anther dehiscence. Shown are the lengths of the gynoecium (D) and long stamens (E) of each flower at the time of stamen excision. For wild type, only flower buds that were not yet open at the time of dissection were used, whereas for the other genotypes, older flowers were also included. Closed symbols indicate gynoecium or stamen lengths of flowers whose excised anthers failed to dehisce; open symbols, gynoecium or stamen lengths of flowers whose excised anthers dehisced. (F-J) Images of turgid anthers at indicated times (minutes) after excision. (K,L) eSEM images of stage 13 anthers taken without freezing the samples at −20°C. Under these conditions, the anthers desiccate and dehisce while under vacuum for microscopy. (M) Time taken to anther dehiscence of turgid anthers excised from stage 13 flowers that matured in high humidity and were then excised in dry conditions. Values are mean time±s.d. until the majority of anthers from a given flower dehisced; *n*=14, 14, 11, 10, 9 and 13 flowers (left to right). Data were compiled from images shown as examples in panels F-J. Letters indicate statistically distinguishable values as assessed by Tukey's HSD test. Fig. S8C shows anther areas from this experiment. Images in A,B,C,F-J are recalculated composites made by the Keyence microscope software from serial images in several consecutive focal planes. Scale bars: 0.2 mm (A,B,F-J), 0.5 mm (C), 0.1 mm (K,L).

Development (2019) 146, dev174375. doi:10.1242/dev.174375

usually dehisced after more than 30 min (Fig. 8M, Fig. S8A). Anthers of the miR167 pathway mutants lost significant volume from their maximal size before desiccation, but were still larger than wild-type anthers at the time they dehisced (Fig. S8B,C). They also generally opened less widely and released less pollen than did wild-type anthers (Fig. 8H,J).

In an attempt to accelerate desiccation without excising stamens, we removed the perianth from stage 12 flower buds on otherwise intact wild-type plants. These anthers dehisced at the normal flower stage when the perianth would have opened (Fig. S7C,D), suggesting that under this condition anthers desiccate less than if excised, and that flower opening per se is not sufficient to trigger dehiscence.

miR167 acts independently of jasmonate response

ARF6 and ARF8 promote jasmonate production at flower stages 11-12, and this burst of jasmonate acts through MYB21 and MYB24 transcription factors to promote filament growth and anther dehiscence. To determine whether this pathway regulates miR167 production, we assayed $P_{MIR167a}$*:GUS* expression in stamens of *aos-2* (jasmonate-deficient), *coi1-1* (jasmonate-insensitive), *myb21 myb24* and *arf6-2 arf8-8* mutant plants (Xie et al., 1998; Reeves et al., 2012; Mlotshwa et al., 2016). Although these flowers lacked jasmonate production or response, and had anthers that arrested at flower stage 11, they each had significant X-Gluc staining in anthers (Fig. 3F,G, Fig. S1B-F). Moreover, qRT-PCR assays showed that miR167 was present in *aos-2* stamens (Fig. S1H). These results indicate that the jasmonate-MYB21 pathway is not required for $P_{MIR167a}$*:GUS* expression and miR167 production in anthers of flower stages 11 and 12.

Anthers of the *aos-2* jasmonate biosynthesis mutant did not normally dehisce (Park et al., 2002; von Malek et al., 2002; Reeves et al., 2012) (Fig. 5H,L, Fig. S3A). In some experiments, *aos-2* anthers were smaller than wild-type indehiscent anthers, perhaps because of shrinkage after stage 13 without dehiscence (Fig. S3A, Fig. 5H,L, Figs S7E and S8D). *aos-2* anthers became competent to dehisce after stamen excision at a later flower stage than did anthers of the other genotypes tested (Fig. 8D,E, Fig. S7F) and they took longer to dehisce than did wild-type anthers after excision from flowers that had opened under high humidity (Fig. 8M, Fig. S8C). *aos-2 mir167a*, *aos-2 mARF6* and *aos-2 mARF8* flowers had short stamen filaments similar to those of *aos-2* plants; and enlarged anthers similar to *mir167a*, *mARF6* or *mARF8* anthers (Figs S3A, S8D,E and S9). *aos-2 mARF8-3/–* anthers usually failed to dehisce even after desiccation (Fig. S7E,F). Lastly, exogenous methyl jasmonate treatment caused *aos-2* and *aos-2 mir167a-1* stamen filaments to elongate and elicited dehiscence of *aos-2* anthers, but did not cause *aos-2 mir167a-1* anthers to dehisce (Fig. S9E-G). Together these results suggest that the anther dehiscence defect caused by loss of mir167 regulation is independent of jasmonate production and response in filaments, although it remains possible that jasmonate response is perturbed in the epidermis of *mir167a* mutant anthers.

DISCUSSION

MIR167a is key for fertility

The close similarity among *mir167a*, *mARF6* and *mARF8* phenotypes indicates that *MIR167a* is the main miR167 precursor gene targeting *ARF6* and *ARF8* transcripts in both anthers and ovules. Consistent with this view, $P_{MIR167a}$*:GUS* is expressed surrounding the anther vasculature at flower stages 11-12 and in developing ovules. Based on expression patterns, three other *MIR167* genes may have functions in other tissues, such as sepals or roots (Wu et al., 2006; Gifford et al., 2008; Medina et al., 2017).

The *mir167a* mutant anther and fertility defects appeared slightly stronger than those of the hemizygous *mARF6/-* or *mARF8/-* plants characterized here, but weaker than those of homozygous *mARF6* or *mARF8* plants. In fact, we detected increased *ARF6* or *ARF8* transcript levels in *mARF6* or *mARF8* stamens, but not in *mir167* mutant stamens. These observations suggest that *mARF* transgene copy number or position effects caused higher levels of *ARF6* or *ARF8* expression than did mutating *MIR167a*. The variable strength of different *mARF6* and *mARF8* lines (Wu et al., 2006) also shows that the dosage of *mARF6* or *mARF8* can affect the timing of anther dehiscence.

miR167 limits anther growth

In *mARF6*, *mARF8* and *mir167a* anthers, ectopic ARF6 and ARF8 promote excess cell expansion growth starting at flower stage 11, ~2 days before flowers open at stage 13 and wild-type anthers normally dehisce. Ectopic ARF6 and ARF8 in cells surrounding the vasculature, where miR167 is normally present (Válóczi et al., 2006; Wu et al., 2006; Rubio-Somoza and Weigel, 2013), likely activate *EXPA8*, *XTH19* and other genes whose products loosen cell walls and thereby increase expansion of perivascular cells.

ARF6 and ARF8 similarly promote cell expansion in hypocotyls, inflorescence stems, petals, stamen filaments and stigma (Nagpal et al., 2005; Ru et al., 2006; Reeves et al., 2012; Reed et al., 2018), and many of the differentially expressed genes in *arf6 arf8* and *mARF8* stamens are also affected by *arf6* mutations in seedlings or are auxin regulated in hypocotyls (Chapman et al., 2012; Oh et al., 2014). Despite this overlap, whereas *SAUR* (small auxin up RNA) genes are the dominant class of genes induced in hypocotyls by auxin or by light conditions that increase auxin production (Chapman et al., 2012; Kohnen et al., 2016; Sun et al., 2016), only one *SAUR* gene (*SAUR42/At2g28085*) was underexpressed in *arf6 arf8* stamens and overexpressed in *mARF8* stamens; and GO and protein domain analyses did not highlight *SAUR* genes in our dataset. This difference might arise if auxin response factors interact with tissue-specific factors to regulate different targets in different tissues.

Although the primary effects of ectopic *ARF6* and *ARF8* likely occur in cells near the central vasculature, cells throughout the anther grew excessively, and expression of the auxin-responsive reporter gene *DR5:GUS* persisted after flower stage 11 in *mARF6* and *mARF8* anthers. *DR5:GUS* is normally expressed in the middle cell layer surrounding anther locules, several cells distant from the location of miR167 action in cells surrounding the vasculature (Válóczi et al., 2006; Wu et al., 2006; Cecchetti et al., 2016). These phenotypes suggest that *MIR167a* has non-cell-autonomous effects on growth and auxin response in anthers. Ectopic *mARF6* transcript was seen only in perivascular cells in anthers (Wu et al., 2006), suggesting that miR167 acts cell-autonomously. While ARF6 and ARF8 proteins might move between cells, *DR5:GUS* is still expressed in P_{35S}*:MIR167a* anthers deficient in both *ARF6* and *ARF8*, indicating that additional transcription factors in anthers can activate this reporter and possibly control growth. Such factors could include other ARF proteins, or targets of brassinolide or gibberellin signaling pathways (Oh et al., 2014). Cells in sepals have variable growth rates that can compensate for each other to result in smooth overall organ growth (Hong et al., 2016), and similar compensation may underlie cell expansion throughout anthers driven by growth of cells in the center. Such effects might be mediated by tension in the tissue deriving from growth of the perivascular cells, increased water availability or other mobile signals.

mir167a and *mARF8* pollen had slightly decreased viability and *in vitro* germination rate, similarly to pollen from inadequately

Development (2019) 146, dev174375. doi:10.1242/dev.174375

desiccated *ice1* mutant anthers (Wei et al., 2018). Delayed desiccation of the anther and its pollen might also delay pollen maturation, or alternatively allow pollen to bypass desiccation and dormancy, as suggested by the occasional pollen germination we observed in *mARF8* anthers. Consistent with either model, many genes characteristic of late stages of pollen maturation were underexpressed in *mARF8* stamens in our RNA-Seq data. It would be interesting to test directly whether anther desiccation induces late-stage pollen gene expression.

Anther growth restriction primes anther dehiscence

We propose that excess anther growth during flower stages 11-12 causes the subsequent dehiscence defect in miR167 pathway mutant anthers because mutant anthers become too large to desiccate efficiently. Some mutant stage 13 anthers had partially open gaps along the stomium, indicating that the cell wall breakdown pathway was likely active, and that even if partially intact at the time of anthesis, the stomium was weakened. In practice, it is difficult to pinpoint the timing of stomium breakage because protocols for microscopy specimen preparation include desiccation steps or vacuum (for eSEM) and chemical fixatives or freezing may not entirely prevent stomium breakage during processing. Several anatomical features appeared normal in the mutants, and, although likely causing faster water loss than normally occurs, stamen excision triggered miR167 pathway mutant anthers to shrink and then dehisce. These results suggest that dehydration limits anther dehiscence, and that these mutants fail to release pollen because they retain too much water.

The delay in desiccation in miR167 pathway mutants might limit production of mechanical forces to crack open the stomium and/or to evert the locule walls to release pollen (Wilson et al., 2011; Nelson et al., 2012; Wei et al., 2018). In this scenario, enlarged mutant anthers could preclude or delay generation of sufficient mechanical force, either because of delayed shrinkage to an appropriate size, or if greater forces are needed to evert the enlarged mutant locule walls than are needed in wild-type anthers. Prolonged hydration might also delay cell wall breakdown in the septum and/or stomium through regulatory pathways regulated by cytoplasmic or apoplastic water potential. Other factors needed for dehiscence such as stomatal differentiation or lignification (Yang et al., 2007; Wei et al., 2018) were apparently unaffected in miR167 pathway mutants. Changes in growth rate are also important for developmental events such as sperm release from pollen, where peptide signals from the female gametophyte induce growth imbalance leading to pollen tube rupture and sperm release (Ge et al., 2017).

Although excess prior growth is likely to be the primary cause of anther indehiscence in plants with defects in miR167 regulation, ectopic ARF6 and ARF8 might continue to act even after flowers open to promote growth and/or impede desiccation, as suggested by the persistent phloem unloading zone in mutant anthers. Increased expression of jasmonate biosynthesis genes and *MYB26* should promote dehiscence, so may be symptoms of delayed desiccation.

Why do wild-type anthers normally dehisce just as flowers open? Perianth removal did not accelerate anther dehiscence in wild-type stage 12 flower buds, suggesting that flower opening per se would not cause sufficient desiccation to induce immediate anther dehiscence. Anther stomata develop at flower stage 12, and *ice1* mutants lacking mature stomata have indehiscent anthers at high relative humidity (Wei et al., 2018), indicating that timing of stomatal development contributes to competence to desiccate and dehisce. Similarly, in the moss *Physcomitrella patens*, stomata contribute to sporophyte capsule rupture (Chater et al., 2016). However, *ice1* mutant anthers did dehisce at low humidity (Wei et al., 2018), suggesting that anthers also lose water by a route that is independent of anther stomata. Water flux through vasculature may slow or even shift from import into anthers to export to other organs, or water may escape through ruptured stomia. *ice1* anthers likely dehisce more readily than do *mir167a* and *mARF6/8* anthers because they do not grow too large and so need to lose less water to open.

Independent action of miR167 and jasmonate

Jasmonate production starting at stage 11 is required to produce dehiscent anthers, and coincides with increased expression of *MIR167a*. However, *MIR167a* is expressed independently of jasmonate production or response, *aos mir167a* double mutants had an additive phenotype, and jasmonate could not rescue *mir167a* anther dehiscence. Finally, jasmonate is thought to be made in the filament and to act in the anther epidermis, whereas miR167 acts in cells surrounding the anther vasculature. These results suggest that miR167 and jasmonate act independently, although it remains possible that miR167 deficiency affects responsiveness to jasmonate specifically in anthers but not in stamen filaments. Signals and factors that initiate contemporaneous jasmonate production in filaments and *MIR167a* expression in anthers might include TCP transcription factors (Schommer et al., 2008; Danisman et al., 2012; Rubio-Somoza and Weigel, 2013).

MATERIALS AND METHODS

Plant material and growth conditions

All plant lines used in this work were in the Columbia (Col-0) ecotype. Most plant seeds were surface sterilized with 95% ethanol followed by bleach solution (2:1 H_2O:bleach with two or three drops of Tween-20), plated on Murashige and Skoog (MS) salts (Murashige and Skoog, 1962) containing 1% (w/v) sucrose and 0.6% (w/v) Phyto-agar (pH 5.7), cold stratified for 1 to 3 days at 4°C, then grown at 22°C with 16-h-light/8-h-dark photoperiod. *mARF6*, *mARF8*, and *mir167a* seeds have defective seed coats and were surface sterilized using 70% (v/v) ethanol, 0.5% (v/v) Triton X-100 (Yadav et al., 2014).

Generation of mutants and promoter fusions

mARF6-A, *mARF8-3* and *mARF8-4* lines were derived using transgene constructs described previously (Wu et al., 2006). *mir167a* mutants were made by CRISPR/Cas9-targeted mutagenesis using the 19-mer sgRNA guide sequence AAAGCTAATTAGATCATGC (Fig. 1K). The guide RNA was cloned into pDONR207 vector (Invitrogen) using primers listed in Table S11, subcloned into binary vector pCUT6 (Peterson et al., 2016) by LR clonase (Invitrogen) and introduced into *Arabidopsis* plants using *Agrobacterium tumefaciens* strain GV3101 by floral dip (Clough, 2005). Basta-resistant T1 transformed plants were selected on soil by spraying with 0.01% Finale (Bayer Environmental Science, RTP, NC) and phenotypic plants identified in the T2 generation. Mutations were identified as having bands of altered mobility on 15% polyacrylamide gels of PCR products using primers listed in Table S11, and by sequencing PCR products spanning the targeted site. The $P_{MIR167a}$*:GUS*, $P_{MIR167c}$*:GUS*, P_{EXPA8}*:GUS*, P_{XTH19}*:GUS*, P_{DR5}*:GUS* and P_{35S}*:MIR167a* constructs and plants were described previously (Ulmasov et al., 1997; Wu et al., 2006; Bassel et al., 2014). To construct P_{SUC2}*:YPET*, a *YPET* open reading frame sequence with an A206K mutation to decrease protein dimerization was amplified by PCR and cloned into pENTR (Invitrogen). This was then recombined by Gateway cloning into a derivative of pB7WG2 destination vector (Karimi et al., 2002) in which the P_{35S} promoter sequences had been replaced with a 2.1 kb upstream promoter sequence from *AtSUC2* (Truernit and Sauer, 1995). The resulting construct was transformed into wild-type Columbia plants, and a line with 3:1 segregation was crossed with *mARF6/−* and *mARF8/−* plants.

Histology and microscopy

Flower X-gluc staining and sectioning of stained anthers were performed as described previously (Ploense et al., 2009). Phloroglucinol staining was

Development (2019) 146, dev174375. doi:10.1242/dev.174375

based on methods described by Mizuno et al. (2007). Wild-type, *mARF6* and *mARF8* mutant flowers at stage 13 were fixed in 3.7% (v/v) formaldehyde, 5% (v/v) acetic acid, 50% (v/v) ethanol at 4°C for 24 h; and dehydrated with an ethanol series [50% (v/v) to 92% (v/v)]. Flowers were stained with 1% (w/v) phloroglucinol (Sigma-Aldrich) in 92% (v/v) ethanol for 5 min and moved to a glass dish, then 25% (v/v) HCl was dropped onto the flowers and stained anthers were photographed.

For microscopy of P_{SUC2}*:YPET* anthers, flowers of phloem loading tracer P_{SUC2}*:YPET* (514 nm excitation; emission collection at 535-600 nm) were washed [1× PBS, 2% (v/v) Tween-20 for 10 min, then 1× PBS] then stained with 0.0005% (w/v) ethidium bromide (560 nm excitation; emission collection at 592-643 nm) (Yang et al., 2007). A weak vacuum was pulled for 30 min, and samples were then left at room temperature for 30 min. Fluorescence was visualized on a Zeiss 710 DUO confocal microscope (Zeiss, Thornwood, NY, USA). Environmental scanning electron microscopy images of anthers were taken on a Hirox SH-3000 mini-SEM microscope (Fig. 4) or a FEI Quanta 200 eSEM (Figs 5 and 8KL, Fig. S4) at 10 kV. Samples for images shown in Figs 4, 5 and Fig. S4 were cooled to −20°C on a cooled specimen stage.

A P_{35S}*:PM-mCherry* transgene with a fusion between *AtPIP2A* and *mCherry* and a Basta-resistance selectable marker gene (Nelson et al., 2007) was transformed into Columbia plants and generously provided by Tim Ross-Elliott (University of North Carolina at Chapel Hill, USA). This line was crossed with *mARF8-3*, and individual F2 plants homozygous for *mARF8-3* and carrying P_{35S}*:PM-mCherry* used for microscopy. For imaging, stamens were immersed in water between glass slide and coverslip separated by 20 µm spacers to prevent tissue crushing. Tiled 1024×1024 pixel images with 2 µm *z*-stack steps were acquired on a Leica TCS sp8 confocal microscope using excitation with a 552 nm solid-state laser and emission detection at 599-641 nm. Tiles were merged and *z*-stack projections generated using LAS X software (Leica Microsystems).

For anther microstructure, first open flowers were fixed in 1.6% paraformaldehyde, 2.5% glutaraldehyde, 50 mM potassium phosphate (pH 6.9), and washed and dehydrated in an ethanol series (Yeung and Chan, 2015). Tissue was embedded in Technovit 7100 resin (Electron Microscopy Sciences, Hatfield, PA) in 0.2 ml thin-walled PCR tubes, cut to 2 µm sections on a Leica JUNG RM2065 rotary microtome with glass knives, stained with 0.5% Toluidine Blue, and observed by light microscopy (Matsushima, 2014; Matsushima et al., 2014; Wei et al., 2018). Ovules were fixed, cleared and observed by differential interference contrast (DIC) microscopy, as described previously (Wu et al., 2006).

For pollen viability assays, a stock solution of 1% Fluorescein diacetate (FDA, Fluka BioChemika 31545) in acetone was diluted 1000× in 20% sucrose just before use. Pollen was released into a drop of diluted FDA by dabbing the anther on the drop on a glass slide, and a coverslip was overlaid. Pollen fluorescence indicating viable pollen was observed under a fluorescence microscope using GFP filters. Pollen germination was assayed as described (Dickinson et al., 2018) with the germination medium buffered at pH 7.5 and using cellophane membrane 95P (Futamura USA, Atlanta, GA).

Photographs and organ measurements

Flowers and floral organs were photographed using a Leica DFC420 camera on a Wild dissecting microscope, and measured from images using ImageJ software or using a camera lucida attachment on the dissecting microscope (Abramoff et al., 2004; Reeves et al., 2012). Some panels in Figs 5B, 6E and 8K, Figs S1 and S6 are composite images of partly overlapping fields stitched together either manually or using the Automate>photomerge function in Photoshop software. Flower and anther images in desiccation experiments were obtained using a Keyence VHX-5000 microscope. Images presented in Fig. 8 are recalculated composites made by the Keyence microscope software from serial images in several consecutive focal planes.

Transcript analyses

Plants were grown in 14:10 h day:night cycles for RNA-Seq experiments or 16:8 h cycles for qRT-PCR. Samples for RNA analyses were collected between 1 and 3 h after dawn and immediately frozen in liquid nitrogen. Stage 11 flower buds were 1.5-1.8 mm long, generally corresponding to flowers −3 to −5. Stamens at this stage still appeared green before turning yellow at flower stage 12. For RNA-Seq, RNA was isolated using the Rneasy Plant Mini kit (Qiagen) according to the manufacturer's instructions. Libraries were constructed with the Truseq mRNA library prep kit (Illumina) according to the manufacturer's instructions. Samples were bar-coded and multiplexed, and sequenced using an Illumina HiSeq 2000 machine with single-end 50 base reads. Library construction and sequencing were performed at the University of North Carolina high-throughput sequencing facility.

For qRT-PCR, total RNA was extracted using Trizol (Invitrogen) as described by the manufacturer. cDNA was synthesized using the A3500 Reverse Transcription System (Promega) according to the manufacturer's instructions. For the mRNA, reverse transcription was conducted using Oligo(dT)15 Primer; for miRNA, reverse transcription used the Stem-loop RT primer (see Table S11). Total RNA of 1 µg was used in a 20 µl volume reaction. The cDNA was diluted 5-fold, and 1 µl was used as a template in a 10 µl PCR reaction. The real-time quantitative RT-PCR was conducted using a DNA Engine Opticon 2 System (Bio-Rad, USA), based on Power SYBR® Green Master Mix (Applied Biosystems). Each 10 µl reaction comprised 1 µl template, 5 µl 2× SYBR Premix, 0.4 µl (10 µM) of each primer and 3.2 µl RNase-free ddH_2O. The primers for transcript analysis were designed using the Primer premier 5.0 software and are listed in Table S11. The reactions were incubated at 95°C for 10 min, followed by 40 cycles of 95°C for 15 s and 60°C for 1 min. A melting curve analysis was performed at the end of the PCR run over the range 60-95°C, increasing the temperature stepwise by 0.2°C every 2 s, normalized to the reference transcript *UBQ10*. Each PCR reaction was carried out in triplicate. C_q values were converted into relative quantities via the delta-C_q method. The amplification efficiencies (E) and correlation coefficient R^2 values were calculated using LinRegPCR software (Karlen et al., 2007; Ruijter et al., 2013).

Bioinformatics analysis

Bioinformatics analyses were performed using a server with two 8-core processors per compute node, 128 gigabytes of RAM, and an Ubuntu Linux-Distribution operating system at the Bioinformatics Research Center (BRC) at North Carolina State University.

Read processing and alignment to the *Arabidopsis* genome

Low-quality cDNA sequences were filtered out with Ea-Utils software (Lindgreen, 2012). Reads with Q-score (phred-like quality score) greater than 20 and read length greater than 20-bp were kept and aligned against the TAIR 10 reference genome (Ensembl annotation) downloaded from the iGenome database (http://support.illumina.com/sequencing/sequencing_software/igenome.html).

TopHat2 (Trapnell et al., 2009), a splice junction mapper, was used to align cleaned reads against the entire *Arabidopsis* genome using the TopHat2 default parameters, except for maximal intron length (−I 2000). The large majority of known introns are smaller than the selected −I 2000 threshold (Li et al., 2013). To align reads solely and exclusively against TAIR 10 annotated gene models, the arguments '−T' (transcriptome only) and '−no-novel-juncs' (no novel junction) also were included. Only uniquely mapped reads to the entire genome were used for downstream analysis. Uniquely mapped reads were extracted from the alignment output binary (BAM) files using Samtools (Li et al., 2009).

Table counts

The HTSeq: analyzing high-throughput sequencing data with Python software (Anders et al., 2015) was used with default parameters except for the 'stranded=no' mode to generate tables-counts. Tables-counts were analyzed with R packages edgeR (Robinson et al., 2010) and DESeq2 (Seyednasrollah et al., 2015).

Differential gene expression (DEGs)

Differential gene expression analyses were carried out using the R packages edgeR, and DESeq2 and Cufflinks program (Love et al., 2014) for DEGs and transcripts. Filters were applied to determine if a gene was detected as a means to enrich for true DEGs, to reduce type I error, and to improve *P*-value adjustment (Bourgon et al., 2010; Pimentel et al., 2014;

Seyednasrollah et al., 2015). The edgeR function 'counts per million' (cpm) (Robinson et al., 2010) was used to discard those genes whose cpm was lower than a threshold of two reads per gene in at least two biological replicates. For Cufflinks, a minimum RPKM of 5 was set for a gene to be expressed, following the criteria of Suzuki et al. (2015).

Acknowledgements
We thank Bob Franks for supporting G.V.; Stéphane Verger, Lucie Riglet, Carrie Donley, Tony Perdue, Alex Davis, and Bill Kier for help with microscopy; Yoan Coudert for use of the Keyence microscope; Olivier Hamant for use of the sp8 confocal microscope; Tim Ross-Elliott for providing the P_{35S}:*PM-mCherry* line; and Marc Nishimura and Zack Nimchuk for vector pCUT6. Some eSEM images were taken at the Chapel Hill Analytical and Nanofabrication Laboratory (CHANL), a member of the North Carolina Research Triangle Nanotechnology Network (RTNN), which is supported by the National Science Foundation (ECCS-1542015) as part of the National Nanotechnology Coordinated Infrastructure (NNCI).

Competing interests
The authors declare no competing or financial interests.

Author contributions
Conceptualization: P.N., J.W.R.; Formal analysis: L.Z., G.V., J.W.R.; Investigation: L.Z., P.N., B.T., L.B., J.W.R.; Writing - original draft: L.Z., G.V., J.W.R.; Writing - review & editing: J.W.R.; Visualization: L.Z., J.W.R.; Supervision: P.N., Y.H., J.W.R.; Project administration: J.W.R.; Funding acquisition: L.Z., J.W.R.

Funding
This work was supported by US National Science Foundation (IOS-1147045 to J.W.R. and P.N.), by a visiting faculty fellowship from the Ecole Normale Supérieure (ENS) to J.W.R., and by a Chinese Government Scholarship to L.Z. Access to the Leica sp8 confocal microscope was possible thanks to a grant from the European Research Council (ERC-2013-CoG-615739 'MechanoDevo' to O. Hamant).

Data availability
RNA-Seq data reported in this article have been deposited in GEO under accession number GSE122436.

Supplementary information
Supplementary information available online at
http://dev.biologists.org/lookup/doi/10.1242/dev.174375.supplemental

References
Abramoff, M. D., Magelhaes, P. J. and Ram, S. J. (2004). Image processing with ImageJ. *Biophoton. Int.* **11**, 36-42.
Aloni, R., Aloni, E., Langhans, M. and Ullrich, C. I. (2006). Role of auxin in regulating Arabidopsis flower development. *Planta* **223**, 315-328. doi:10.1007/s00425-005-0088-9
Anders, S., Pyl, P. T. and Huber, W. (2015). HTSeq–a Python framework to work with high-throughput sequencing data. *Bioinformatics* **31**, 166-169. doi:10.1093/bioinformatics/btu638
Bassel, G. W., Stamm, P., Mosca, G., Barbier de Reuille, P., Gibbs, D. J., Winter, R., Janka, A., Holdsworth, M. J. and Smith, R. S. (2014). Mechanical constraints imposed by 3D cellular geometry and arrangement modulate growth patterns in the Arabidopsis embryo. *Proc. Natl. Acad. Sci. USA* **111**, 8685-8690. doi:10.1073/pnas.1404616111
Bourgon, R., Gentleman, R. and Huber, W. (2010). Independent filtering increases detection power for high-throughput experiments. *Proc. Natl. Acad. Sci. USA* **107**, 9546-9551. doi:10.1073/pnas.0914005107
Cecchetti, V., Altamura, M. M., Falasca, G., Costantino, P. and Cardarelli, M. (2008). Auxin regulates Arabidopsis anther dehiscence, pollen maturation, and filament elongation. *Plant Cell* **20**, 1760-1774. doi:10.1105/tpc.107.057570
Cecchetti, V., Altamura, M. M., Brunetti, P., Petrocelli, V., Falasca, G., Ljung, K., Costantino, P. and Cardarelli, M. (2013). Auxin controls Arabidopsis anther dehiscence by regulating endothecium lignification and jasmonic acid biosynthesis. *Plant J.* **74**, 411-422. doi:10.1111/tpj.12130
Cecchetti, V., Brunetti, P., Napoli, N., Fattorini, L., Altamura, M. M., Costantino, P. and Cardarelli, M. (2015). ABCB1 and ABCB19 auxin transporters have synergistic effects on early and late Arabidopsis anther development. *J. Integr. Plant Biol.* **57**, 1089-1098. doi:10.1111/jipb.12332
Cecchetti, V., Celebrin, D., Napoli, N., Ghelli, R., Brunetti, P., Costantino, P. and Cardarelli, M. (2016). An auxin maximum in the middle layer controls stamen development and pollen maturation in Arabidopsis. *New Phytol.* **213**, 1194-1207. doi:10.1111/nph.14207
Chapman, E. J., Greenham, K., Castillejo, C., Sartor, R., Bialy, A., Sun, T.-P. and Estelle, M. (2012). Hypocotyl transcriptome reveals auxin regulation of growth-promoting genes through GA-dependent and -independent pathways. *PLoS ONE* **7**, e36210. doi:10.1371/journal.pone.0036210
Chater, C. C., Caine, R. S., Tomek, M., Wallace, S., Kamisugi, Y., Cuming, A. C., Lang, D., MacAlister, C. A., Casson, S., Bergmann, D. C. et al. (2016). Origin and function of stomata in the moss Physcomitrella patens. *Nat. Plants* **2**, 16179. doi:10.1038/nplants.2016.179
Cheng, H., Song, S., Xiao, L., Soo, H. M., Cheng, Z., Xie, D. and Peng, J. (2009). Gibberellin acts through jasmonate to control the expression of MYB21, MYB24, and MYB57 to promote stamen filament growth in Arabidopsis. *PLoS Genet.* **5**, e1000440. doi:10.1371/journal.pgen.1000440
Clough, S. J. (2005). Floral dip: agrobacterium-mediated germ line transformation. *Methods Mol. Biol.* **286**, 91-102.
Cosgrove, D. J. (2016). Plant cell wall extensibility: connecting plant cell growth with cell wall structure, mechanics, and the action of wall-modifying enzymes. *J. Exp. Bot.* **67**, 463-476. doi:10.1093/jxb/erv511
Danisman, S., van der Wal, F., Dhondt, S., Waites, R., de Folter, S., Bimbo, A., van Dijk, A. D., Muino, J. M., Cutri, L., Dornelas, M. C. et al. (2012). Arabidopsis class I and class II TCP transcription factors regulate jasmonic acid metabolism and leaf development antagonistically. *Plant Physiol.* **159**, 1511-1523. doi:10.1104/pp.112.200303
Dickinson, H., Rodriguez-Enriquez, J. and Grant-Downton, R. (2018). Pollen Germination and Pollen Tube Growth of Arabidopsis thaliana: in vitro and Semi in vivo Methods. *BioProtocol* **8**, e2977. doi:10.21769/BioProtoc.2977
Feys, B. J. F., Benedetti, C. E., Penfold, C. N. and Turner, J. G. (1994). Arabidopsis mutants selected for resistance to the Phytotoxin Coronatine are male sterile, insensitive to methyl jasmonate, and resistant to a bacterial pathogen. *Plant Cell* **6**, 751-759. doi:10.1105/tpc.6.5.751
Ge, Z., Bergonci, T., Zhao, Y., Zou, Y., Du, S., Liu, M.-C., Luo, X., Ruan, H., García-Valencia, L. E., Zhong, S. et al. (2017). Arabidopsis pollen tube integrity and sperm release are regulated by RALF-mediated signaling. *Science* **358**, 1596-1600. doi:10.1126/science.aao3642
Gifford, M. L., Dean, A., Gutierrez, R. A., Coruzzi, G. M. and Birnbaum, K. D. (2008). Cell-specific nitrogen responses mediate developmental plasticity. *Proc. Natl. Acad. Sci. USA* **105**, 803-808. doi:10.1073/pnas.0709559105
Hong, L., Dumond, M., Tsugawa, S., Sapala, A., Routier-Kierzkowska, A.-L., Zhou, Y., Chen, C., Kiss, A., Zhu, M., Hamant, O. et al. (2016). Variable cell growth yields reproducible organ development through spatiotemporal averaging. *Dev. Cell* **38**, 15-32. doi:10.1016/j.devcel.2016.06.016
Honys, D. and Twell, D. (2004). Transcriptome analysis of haploid male gametophyte development in Arabidopsis. *Genome Biol.* **5**, R85. doi:10.1186/gb-2004-5-11-r85
Huang, H., Gao, H., Liu, B., Qi, T., Tong, J., Xiao, L., Xie, D. and Song, S. (2017). Arabidopsis MYB24 regulates jasmonate-mediated stamen development. *Front. Plant Sci.* **8**, 1525. doi:10.3389/fpls.2017.01525
Imlau, A., Truernit, E. and Sauer, N. (1999). Cell-to-cell and long-distance trafficking of the green fluorescent protein in the phloem and symplastic unloading of the protein into sink tissues. *Plant Cell* **11**, 309-322. doi:10.1105/tpc.11.3.309
Ishiguro, S., Kawai-Oda, A., Ueda, J., Nishida, I. and Okada, K. (2001). The DEFECTIVE IN ANTHER DEHISCIENCE gene encodes a novel phospholipase A1 catalyzing the initial step of jasmonic acid biosynthesis, which synchronizes pollen maturation, anther dehiscence, and flower opening in Arabidopsis. *Plant Cell* **13**, 2191-2209. doi:10.1105/tpc.13.10.2191
Jewell, J. B. and Browse, J. (2016). Epidermal jasmonate perception is sufficient for all aspects of jasmonate-mediated male fertility in Arabidopsis. *Plant J.* **85**, 634-647. doi:10.1111/tpj.13131
Karimi, M., Inzé, D. and Depicker, A. (2002). GATEWAY™ vectors for Agrobacterium-mediated plant transformation. *Trends Plant Sci.* **7**, 193-195. doi:10.1016/S1360-1385(02)02251-3
Karlen, Y., McNair, A., Perseguers, S., Mazza, C. and Mermod, N. (2007). Statistical significance of quantitative PCR. *BMC Bioinformatics* **8**, 131. doi:10.1186/1471-2105-8-131
Kerk, D., Bulgrien, J., Smith, D. W. and Gribskov, M. (2003). Arabidopsis proteins containing similarity to the universal stress protein domain of bacteria. *Plant Physiol.* **131**, 1209-1219. doi:10.1104/pp.102.016006
Kohnen, M. V., Schmid-Siegert, E., Trevisan, M., Petrolati, L. A., Sénéchal, F., Müller-Moulé, P., Maloof, J., Xenarios, I. and Fankhauser, C. (2016). Neighbor detection induces organ-specific transcriptomes, revealing patterns underlying hypocotyl-specific growth. *Plant Cell* **28**, 2889-2904. doi:10.1105/tpc.16.00463
Li, L., Zhao, Y., McCaig, B. C., Wingerd, B. A., Wang, J., Whalon, M. E., Pichersky, E. and Howe, G. A. (2004). The tomato homolog of CORONATINE-INSENSITIVE1 is required for the maternal control of seed maturation, jasmonate-signaled defense responses, and glandular trichome development. *Plant Cell* **16**, 126-143. doi:10.1105/tpc.017954
Li, H., Handsaker, B., Wysoker, A., Fennell, T., Ruan, J., Homer, N., Marth, G., Abecasis, G. and Durbin, R. (2009). The sequence alignment/Map format and SAMtools. *Bioinformatics* **25**, 2078-2079. doi:10.1093/bioinformatics/btp352
Li, S., Liberman, L. M., Mukherjee, N., Benfey, P. N. and Ohler, U. (2013). Integrated detection of natural antisense transcripts using strand-specific RNA sequencing data. *Genome Res.* **23**, 1730-1739. doi:10.1101/gr.149310.112

Lindgreen, S. (2012). AdapterRemoval: easy cleaning of next generation sequencing reads. *BMC Res. Notes* **5**, 337. doi:10.1186/1756-0500-5-337
Liu, N., Wu, S., Van Houten, J., Wang, Y., Ding, B., Fei, Z., Clarke, T. H., Reed, J. W. and van der Knaap, E. (2014). Down-regulation of AUXIN RESPONSE FACTORS 6 and 8 by microRNA 167 leads to floral development defects and female sterility in tomato. *J. Exp. Bot.* **65**, 2507-2520. doi:10.1093/jxb/eru141
Love, M. I., Huber, W. and Anders, S. (2014). Moderated estimation of fold change and dispersion for RNA-seq data with DESeq2. *Genome Biol.* **15**, 550. doi:10.1186/s13059-014-0550-8
Mandaokar, A., Thines, B., Shin, B., Lange, B. M., Choi, G., Koo, Y. J., Yoo, Y. J., Choi, Y. D. and Browse, J. (2006). Transcriptional regulators of stamen development in Arabidopsis identified by transcriptional profiling. *Plant J.* **46**, 984-1008. doi:10.1111/j.1365-313X.2006.02756.x
Matsushima, R. (2014). Thin Sections of Technovit 7100 resin of rice endosperm and staining. *Bio-Protocol* **4**, e1239. doi:10.21769/BioProtoc.1239
Matsushima, R., Maekawa, M., Kusano, M., Kondo, H., Fujita, N., Kawagoe, Y. and Sakamoto, W. (2014). Amyloplast-localized SUBSTANDARD STARCH GRAIN4 protein influences the size of starch grains in rice endosperm. *Plant Physiol.* **164**, 623-636. doi:10.1104/pp.113.229591
Mecchia, M. A., Santos-Fernandez, G., Duss, N. N., Somoza, S. C., Boisson-Dernier, A., Gagliardini, V., Martínez-Bernardini, A., Fabrice, T. N., Ringli, C., Muschietti, J. P. et al. (2017). RALF4/19 peptides interact with LRX proteins to control pollen tube growth in Arabidopsis. *Science* **358**, 1600-1603. doi:10.1126/science.aao5467
Medina, C., da Rocha, M., Magliano, M., Ratpopoulo, A., Revel, B., Marteu, N., Magnone, V., Lebrigand, K., Cabrera, J., Barcala, M. et al. (2017). Characterization of microRNAs from Arabidopsis galls highlights a role for miR159 in the plant response to the root-knot nematode Meloidogyne incognita. *New Phytol.* **216**, 882-896. doi:10.1111/nph.14717
Mizuno, S., Osakabe, Y., Maruyama, K., Ito, T., Osakabe, K., Sato, T., Shinozaki, K. and Yamaguchi-Shinozaki, K. (2007). Receptor-like protein kinase 2 (RPK 2) is a novel factor controlling anther development in Arabidopsis thaliana. *Plant J.* **50**, 751-766. doi:10.1111/j.1365-313X.2007.03083.x
Mlotshwa, S., Pruss, G. J., MacArthur, J. L., Reed, J. W. and Vance, V. (2016). Developmental defects mediated by the P1/HC-pro potyviral silencing suppressor are not due to misregulation of AUXIN RESPONSE FACTOR 8. *Plant Physiol.* **172**, 1853-1861. doi:10.1104/pp.16.01030
Murashige, T. and Skoog, F. (1962). A revised medium for rapid growth and bioassays with tobacco tissue cultures. *Physiol. Plant* **15**, 473-497. doi:10.1111/j.1399-3054.1962.tb08052.x
Murphy, E. and De Smet, I. (2014). Understanding the RALF family: a tale of many species. *Trends Plant Sci.* **19**, 664-671. doi:10.1016/j.tplants.2014.06.005
Nagpal, P., Ellis, C. M., Weber, H., Ploense, S. E., Barkawi, L. S., Guilfoyle, T. J., Hagen, G., Alonso, J. M., Cohen, J. D., Farmer, E. E. et al. (2005). Auxin response factors ARF6 and ARF8 promote jasmonic acid production and flower maturation. *Development* **132**, 4107-4118. doi:10.1242/dev.01955
Nelson, B. K., Cai, X. and Nebenführ, A. (2007). A multicolored set of in vivo organelle markers for co-localization studies in Arabidopsis and other plants. *Plant J.* **51**, 1126-1136. doi:10.1111/j.1365-313X.2007.03212.x
Nelson, M. R., Band, L. R., Dyson, R. J., Lessinnes, T., Wells, D. M., Yang, C., Everitt, N. M., Jensen, O. E. and Wilson, Z. A. (2012). A biomechanical model of anther opening reveals the roles of dehydration and secondary thickening. *New Phytol.* **196**, 1030-1037. doi:10.1111/j.1469-8137.2012.04329.x
Oh, E., Zhu, J.-Y., Bai, M.-Y., Arenhart, R. A., Sun, Y. and Wang, Z.-Y. (2014). Cell elongation is regulated through a central circuit of interacting transcription factors in the Arabidopsis hypocotyl. *eLife* **3**, e03031. doi:10.7554/eLife.03031
Park, J.-H., Halitschke, R., Kim, H. B., Baldwin, I. T., Feldmann, K. A. and Feyereisen, R. (2002). A knock-out mutation in allene oxide synthase results in male sterility and defective wound signal transduction in Arabidopsis due to a block in jasmonic acid biosynthesis. *Plant J.* **31**, 1-12. doi:10.1046/j.1365-313X.2002.01328.x
Peterson, B. A., Haak, D. C., Nishimura, M. T., Teixeira, P. J. P. L., James, S. R., Dangl, J. L. and Nimchuk, Z. L. (2016). Genome-wide assessment of efficiency and specificity in CRISPR/Cas9 mediated multiple site targeting in arabidopsis. *PLoS ONE* **11**, e0162169. doi:10.1371/journal.pone.0162169
Pimentel, H., Parra, M., Gee, S., Ghanem, D., An, X., Li, J., Mohandas, N., Pachter, L. and Conboy, J. G. (2014). A dynamic alternative splicing program regulates gene expression during terminal erythropoiesis. *Nucleic Acids Res.* **42**, 4031-4042. doi:10.1093/nar/gkt1388
Ploense, S. E., Wu, M.-F., Nagpal, P. and Reed, J. W. (2009). A gain-of-function mutation in IAA18 alters Arabidopsis embryonic apical patterning. *Development* **136**, 1509-1517. doi:10.1242/dev.025932
Qi, T., Huang, H., Song, S. and Xie, D. (2015). Regulation of Jasmonate-mediated stamen development and seed production by a bHLH-MYB complex in arabidopsis. *Plant Cell* **27**, 1620-1633. doi:10.1105/tpc.15.00116
Reed, J. W., Wu, M.-F., Reeves, P. H., Hodgens, C., Yadav, V., Hayes, S. and Pierik, R. (2018). Three auxin response factors promote hypocotyl elongation. *Plant Physiol.* **178**, 864-875. doi:10.1104/pp.18.00718
Reeves, P. H., Ellis, C. M., Ploense, S. E., Wu, M.-F., Yadav, V., Tholl, D., Chételat, A., Haupt, I., Kennerley, B. J., Hodgens, C. et al. (2012). A regulatory network for coordinated flower maturation. *PLoS Genet.* **8**, e1002506. doi:10.1371/journal.pgen.1002506
Robinson, M. D., McCarthy, D. J. and Smyth, G. K. (2010). edgeR: a Bioconductor package for differential expression analysis of digital gene expression data. *Bioinformatics* **26**, 139-140. doi:10.1093/bioinformatics/btp616
Ru, P., Xu, L., Ma, H. and Huang, H. (2006). Plant fertility defects induced by the enhanced expression of microRNA167. *Cell Res.* **16**, 457-465. doi:10.1038/sj.cr.7310057
Rubio-Somoza, I. and Weigel, D. (2013). Coordination of flower maturation by a regulatory circuit of three microRNAs. *PLoS Genet.* **9**, e1003374. doi:10.1371/journal.pgen.1003374
Ruijter, J. M., Pfaffl, M. W., Zhao, S., Spiess, A. N., Boggy, G., Blom, J., Rutledge, R. G., Sisti, D., Lievens, A., De Preter, K. et al. (2013). Evaluation of qPCR curve analysis methods for reliable biomarker discovery: bias, resolution, precision, and implications. *Methods* **59**, 32-46. doi:10.1016/j.ymeth.2012.08.011
Salazar-Iribe, A., Agredano-Moreno, L. T., Zúñiga-Sánchez, E., Jiménez-Garcia, L. F. and Gamboa-deBuen, A. (2016). The cell wall DUF642 At2g41800 (TEB) protein is involved in hypocotyl cell elongation. *Plant Sci.* **253**, 206-214. doi:10.1016/j.plantsci.2016.10.007
Sanders, P. M., Lee, P. Y., Biesgen, C., Boone, J. D., Beals, T. P., Weiler, E. W. and Goldberg, R. B. (2000). The arabidopsis DELAYED DEHISCENCE1 gene encodes an enzyme in the jasmonic acid synthesis pathway. *Plant Cell* **12**, 1041-1062. doi:10.1105/tpc.12.7.1041
Schommer, C., Palatnik, J. F., Aggarwal, P., Chételat, A., Cubas, P., Farmer, E. E., Nath, U. and Weigel, D. (2008). Control of jasmonate biosynthesis and senescence by miR319 targets. *PLoS Biol.* **6**, e230. doi:10.1371/journal.pbio.0060230
Schubert, R., Dobritzsch, S., Gruber, C., Hause, G., Athmer, B., Schreiber, T., Marillonnet, S., Okabe, Y., Ezura, H., Acosta, I. F. et al. (2019). Tomato MYB21 acts in ovules to mediate Jasmonate-regulated fertility. *Plant Cell* **31**, 1043-1062. doi:10.1105/tpc.18.00978
Seyednasrollah, F., Laiho, A. and Elo, L. L. (2015). Comparison of software packages for detecting differential expression in RNA-seq studies. *Brief. Bioinform.* **16**, 59-70. doi:10.1093/bib/bbt086
Smyth, D. R., Bowman, J. L. and Meyerowitz, E. M. (1990). Early flower development in Arabidopsis. *Plant Cell* **2**, 755-767. doi:10.1105/tpc.2.8.755
Song, S., Qi, T., Huang, H., Ren, Q., Wu, D., Chang, C., Peng, W., Liu, Y., Peng, J. and Xie, D. (2011). The Jasmonate-ZIM domain proteins interact with the R2R3-MYB transcription factors MYB21 and MYB24 to affect Jasmonate-regulated stamen development in Arabidopsis. *Plant Cell* **23**, 1000-1013. doi:10.1105/tpc.111.083089
Song, S., Chen, Y., Liu, L., See, Y. H. B., Mao, C., Gan, Y. and Yu, H. (2018). OsFTIP7 determines auxin-mediated anther dehiscence in rice. *Nat. Plants* **4**, 495-504. doi:10.1038/s41477-018-0175-0
Stadler, R., Lauterbach, C. and Sauer, N. (2005a). Cell-to-cell movement of green fluorescent protein reveals post-phloem transport in the outer integument and identifies symplastic domains in Arabidopsis seeds and embryos. *Plant Physiol.* **139**, 701-712. doi:10.1104/pp.105.065607
Stadler, R., Wright, K. M., Lauterbach, C., Amon, G., Gahrtz, M., Feuerstein, A., Oparka, K. J. and Sauer, N. (2005b). Expression of GFP-fusions in Arabidopsis companion cells reveals non-specific protein trafficking into sieve elements and identifies a novel post-phloem domain in roots. *Plant J.* **41**, 319-331. doi:10.1111/j.1365-313X.2004.02298.x
Sun, N., Wang, J., Gao, Z., Dong, J., He, H., Terzaghi, W., Wei, N., Deng, X. W. and Chen, H. (2016). Arabidopsis SAURs are critical for differential light regulation of the development of various organs. *Proc. Natl. Acad. Sci. USA* **113**, 6071-6076. doi:10.1073/pnas.1604782113
Suzuki, A., Matsushima, K., Makinoshima, H., Sugano, S., Kohno, T., Tsuchihara, K. and Suzuki, Y. (2015). Single-cell analysis of lung adenocarcinoma cell lines reveals diverse expression patterns of individual cells invoked by a molecular target drug treatment. *Genome Biol.* **16**, 66. doi:10.1186/s13059-015-0636-y
Sze, H., Padmanaban, S., Cellier, F., Honys, D., Cheng, N. H., Bock, K. W., Conejero, G., Li, X., Twell, D., Ward, J. M. et al. (2004). Expression patterns of a novel AtCHX gene family highlight potential roles in osmotic adjustment and K+ homeostasis in pollen development. *Plant Physiol.* **136**, 2532-2547. doi:10.1104/pp.104.046003
Tabata, R., Ikezaki, M., Fujibe, T., Aida, M., Tian, C.-E., Ueno, Y., Yamamoto, K. T., Machida, Y., Nakamura, K. and Ishiguro, S. (2010). Arabidopsis auxin response factor6 and 8 regulate jasmonic acid biosynthesis and floral organ development via repression of class 1 KNOX genes. *Plant Cell Physiol.* **51**, 164-175. doi:10.1093/pcp/pcp176
Trapnell, C., Pachter, L. and Salzberg, S. L. (2009). TopHat: discovering splice junctions with RNA-Seq. *Bioinformatics* **25**, 1105-1111. doi:10.1093/bioinformatics/btp120
Truernit, E. and Sauer, N. (1995). The promoter of the Arabidopsis thaliana SUC2 sucrose-H+ symporter gene directs expression of beta-glucuronidase to the phloem: evidence for phloem loading and unloading by SUC2. *Planta* **196**, 564-570. doi:10.1007/BF00203657

Ulmasov, T., Hagen, G. and Guilfoyle, T. J. (1997). ARF1, a transcription factor that binds to auxin response elements. *Science* **276**, 1865-1868. doi:10.1126/science.276.5320.1865

Ulmasov, T., Hagen, G. and Guilfoyle, T. J. (1999). Activation and repression of transcription by auxin-response factors. *Proc. Natl. Acad. Sci. USA* **96**, 5844-5849. doi:10.1073/pnas.96.10.5844

Válóczi, A., Várallyay, E., Kauppinen, S., Burgyán, J. and Havelda, Z. (2006). Spatio-temporal accumulation of microRNAs is highly coordinated in developing plant tissues. *Plant J.* **47**, 140-151. doi:10.1111/j.1365-313X.2006.02766.x

Verelst, W., Saedler, H. and Munster, T. (2007a). MIKC* MADS-protein complexes bind motifs enriched in the proximal region of late pollen-specific Arabidopsis promoters. *Plant Physiol.* **143**, 447-460. doi:10.1104/pp.106.089805

Verelst, W., Twell, D., de Folter, S., Immink, R., Saedler, H. and Münster, T. (2007b). MADS-complexes regulate transcriptome dynamics during pollen maturation. *Genome Biol.* **8**, R249. doi:10.1186/gb-2007-8-11-r249

von Malek, B., van der Graaff, E., Schneitz, K. and Keller, B. (2002). The Arabidopsis male-sterile mutant dde2-2 is defective in the ALLENE OXIDE SYNTHASE gene encoding one of the key enzymes of the jasmonic acid biosynthesis pathway. *Planta* **216**, 187-192. doi:10.1007/s00425-002-0906-2

Wang, Y., Zhang, W.-Z., Song, L.-F., Zou, J.-J., Su, Z. and Wu, W.-H. (2008). Transcriptome analyses show changes in gene expression to accompany pollen germination and tube growth in Arabidopsis. *Plant Physiol.* **148**, 1201-1211. doi:10.1104/pp.108.126375

Wei, D., Liu, M., Chen, H., Zheng, Y., Liu, Y., Wang, X., Yang, S., Zhou, M. and Lin, J. (2018). INDUCER OF CBF EXPRESSION 1 is a male fertility regulator impacting anther dehydration in Arabidopsis. *PLoS Genet.* **14**, e1007695. doi:10.1371/journal.pgen.1007695

Wilson, Z. A., Song, J., Taylor, B. and Yang, C. (2011). The final split: the regulation of anther dehiscence. *J. Exp. Bot.* **62**, 1633-1649. doi:10.1093/jxb/err014

Wu, M.-F., Tian, Q. and Reed, J. W. (2006). *Arabidopsis microRNA167* controls patterns of *ARF6* and *ARF8* expression, and regulates both female and male reproduction. *Development* **133**, 4211-4218. doi:10.1242/dev.02602

Xie, D. X., Feys, B. F., James, S., Nieto-Rostro, M. and Turner, J. G. (1998). COI1: an Arabidopsis gene required for jasmonate-regulated defense and fertility. *Science* **280**, 1091-1094. doi:10.1126/science.280.5366.1091

Yadav, Y., Molina, I., Ranathunge, K., Queralta Castillo, I., Rothstein, S. J. and Reed, J. W. (2014). ABCG transporters are required for suberin and pollen wall extracellular barriers in *Arabidopsis*. *Plant Cell* **26**, 3569-3588. doi:10.1105/tpc.114.129049

Yang, C., Xu, Z., Song, J., Conner, K., Vizcay Barrena, G. and Wilson, Z. A. (2007). Arabidopsis MYB26/MALE STERILE35 regulates secondary thickening in the endothecium and is essential for anther dehiscence. *Plant Cell* **19**, 534-548. doi:10.1105/tpc.106.046391

Yeung, E. C. and Chan, C. K. W. (2015). Glycol methacrylate: the art of embedding and serial sectioning. *Botany* **93**, 1-8. doi:10.1139/cjb-2014-0177

Zúñiga-Sánchez, E., Soriano, D., Martinez-Barajas, E., Orozco-Segovia, A. and Gamboa-deBuen, A. (2014). BIIDXI, the At4g32460 DUF642 gene, is involved in pectin methyl esterase regulation during Arabidopsis thaliana seed germination and plant development. *BMC Plant Biol.* **14**, 338. doi:10.1186/s12870-014-0338-8

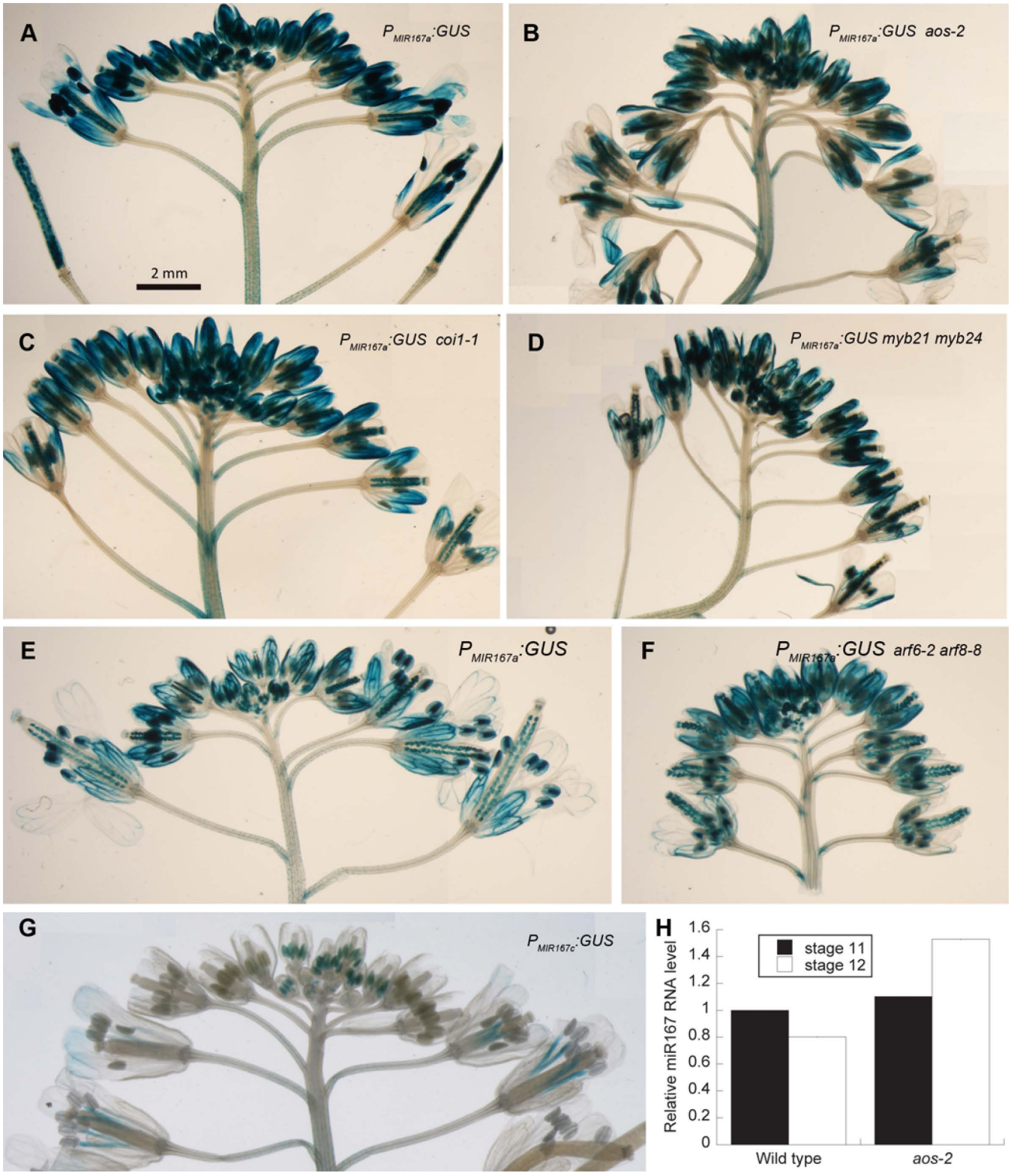

Figure S1. *$P_{MIR167A}$:GUS* and *$P_{MIR167C}$:GUS* X-Gluc staining.

A-F) *$P_{MIR167a}$:GUS* whole inflorescences

G) *$P_{MIR167C}$:GUS* inflorescence.

Panels A-E and G show composite images obtained by splicing together multiple images from different portions of the specimen.

H) qRT-PCR of miR167 in wild-type and *aos-2* stamens at stages 11 and 12. A replicate experiment with pooled tissue from stages 11-13 also showed very similar values in wild-type and *aos-2* stamens.

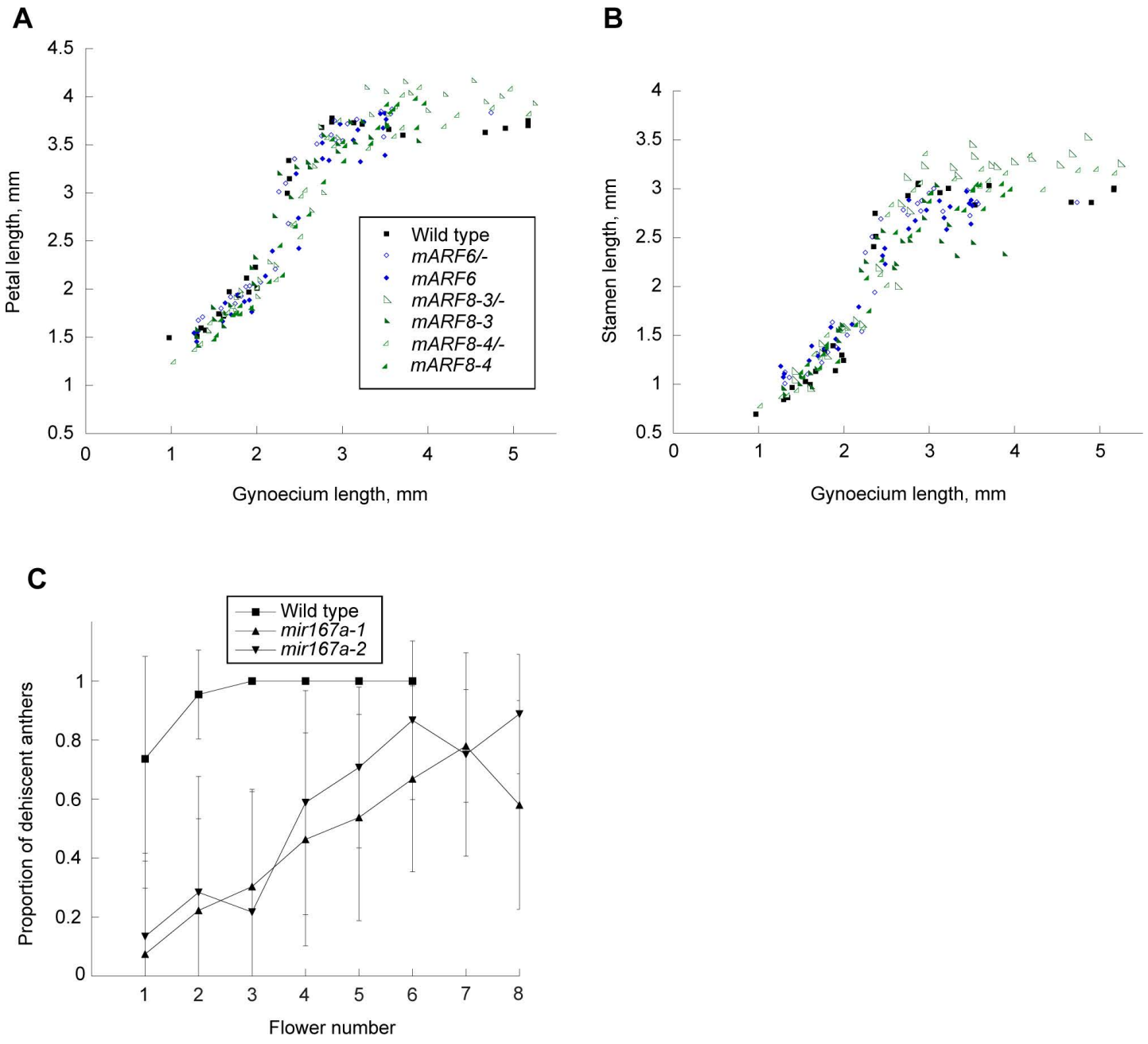

Figure S2. Flower organ lengths s of *mARF6* and *mARF8* lines and dehiscence of *mir167a* mutant anthers.

A,B) Flower organ measurements in homozygous and hemizygous *mARF6* and *mARF8* flowers. A) Petals. B) Stamens. Gynoecium lengths were used as an internal reference for the stage flower maturation.

C) Proportion of dehiscent anthers in wild-type *mir167a-1*, and *mir167a-2* anthers on intact plants.

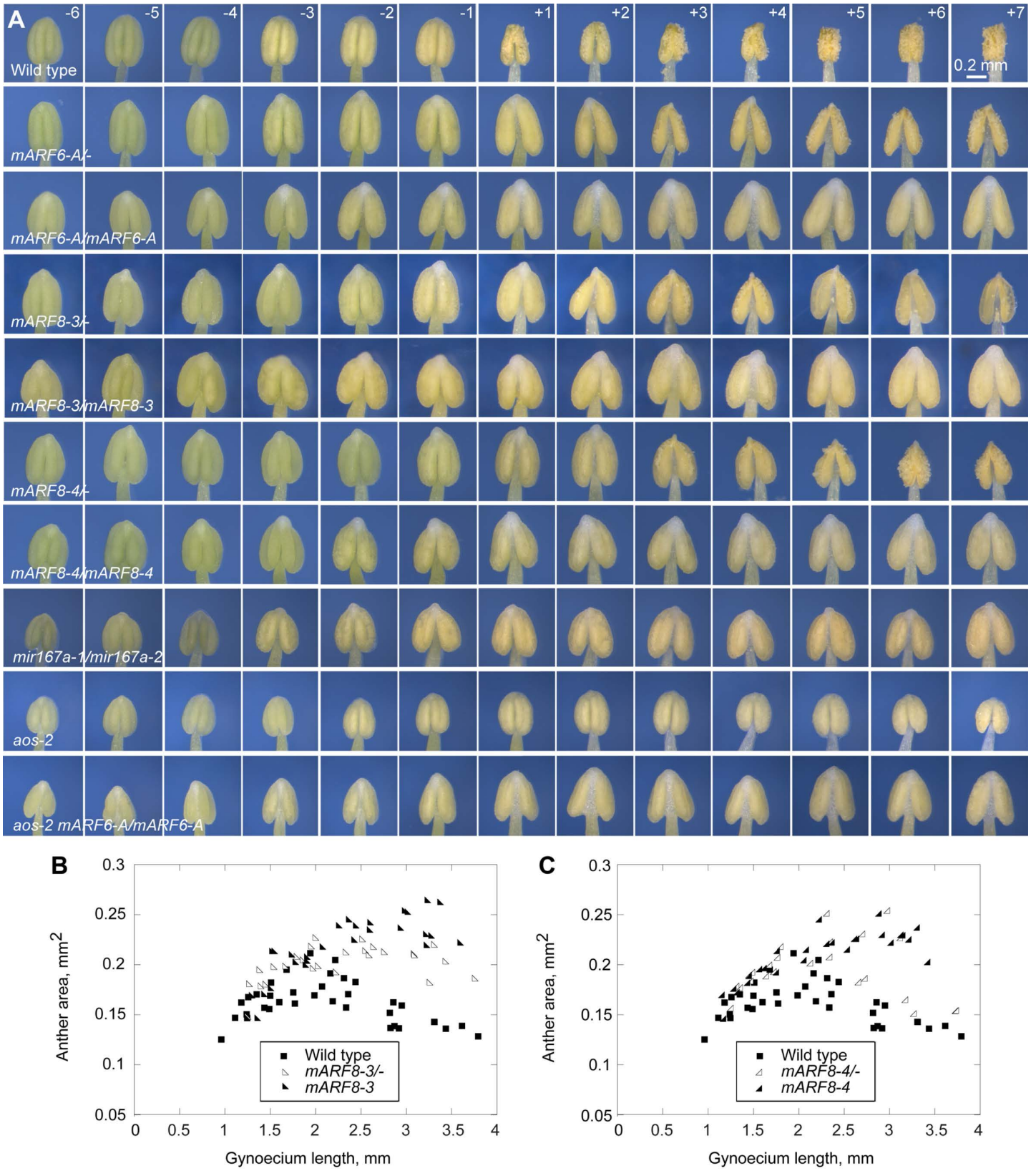

Figure S3. Anther growth phenotypes.

A) A thers from 13 consecutive flowers from individual apices of indicated genotypes. Flower -1 is the largest closed bud, and flower +1 is the first open flower.

B) A ther measurements for *mARF8* flowers. Figure 4 shows data for *mARF6* flowers.

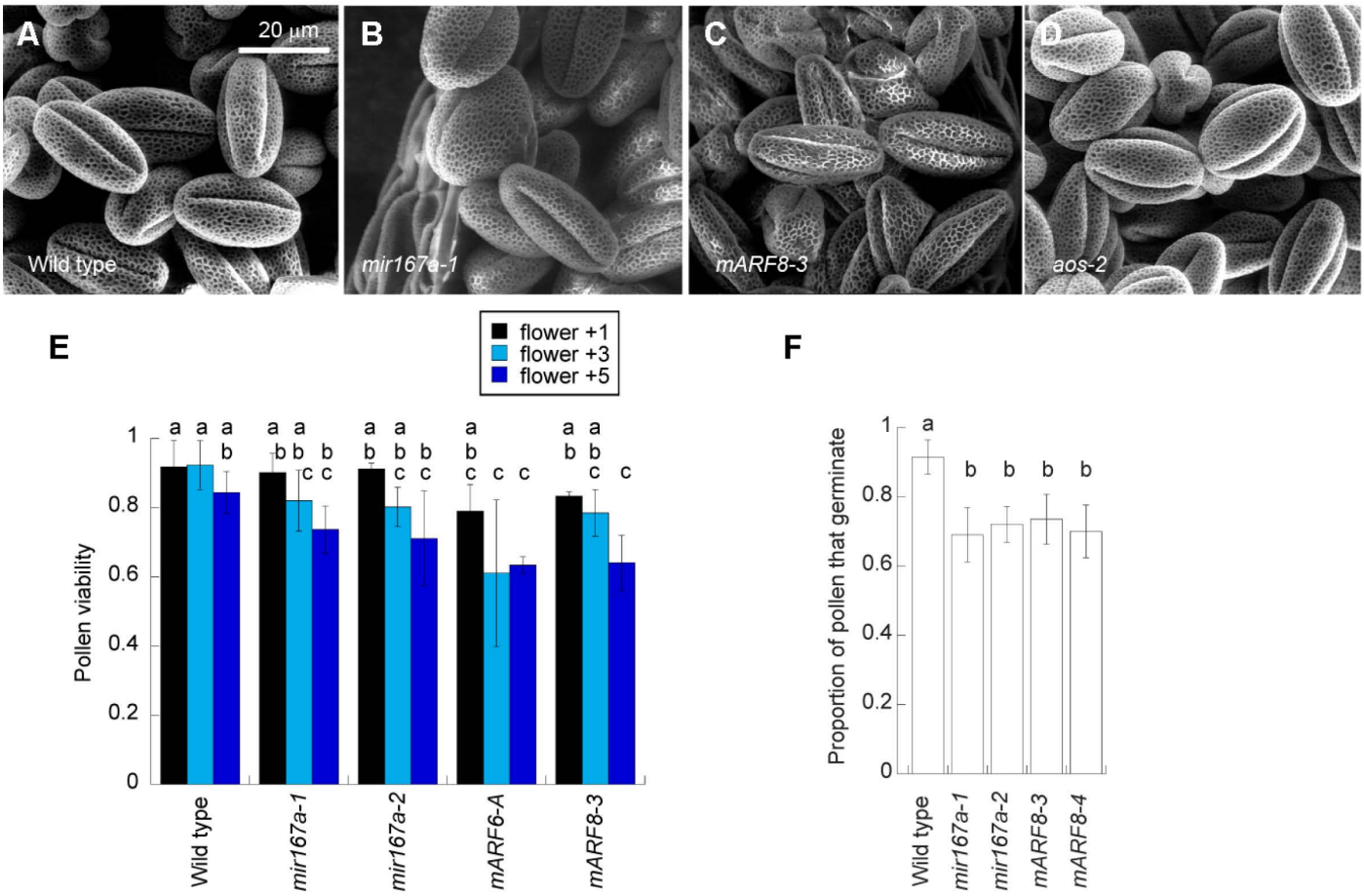

Figure S4. Characterization of *mir167a* and *mARF* pollen.
A-D) eSEM images of pollen from indicated genotypes. Scale bar = 20 µm.
E) Viability of pollen from indicated genotypes at flowers +1, +3, and +5, as indicated by FDA staining.
n=3-7 flowers per genotype, 120-280 pollen grains per sample.
F) Proportion of pollen that germinated in vitro of indicated genotypes. Pollen was taken from flowers +1 or +5.
As the germination rates for these two flower stages did not differ, the data for both were combined in the graph.
n=6-12 flowers per genotype, 230-500 pollen grains per sample.
In E and F, letters indicate statistical classes based on Tukey's Honestly Significant Difference test.

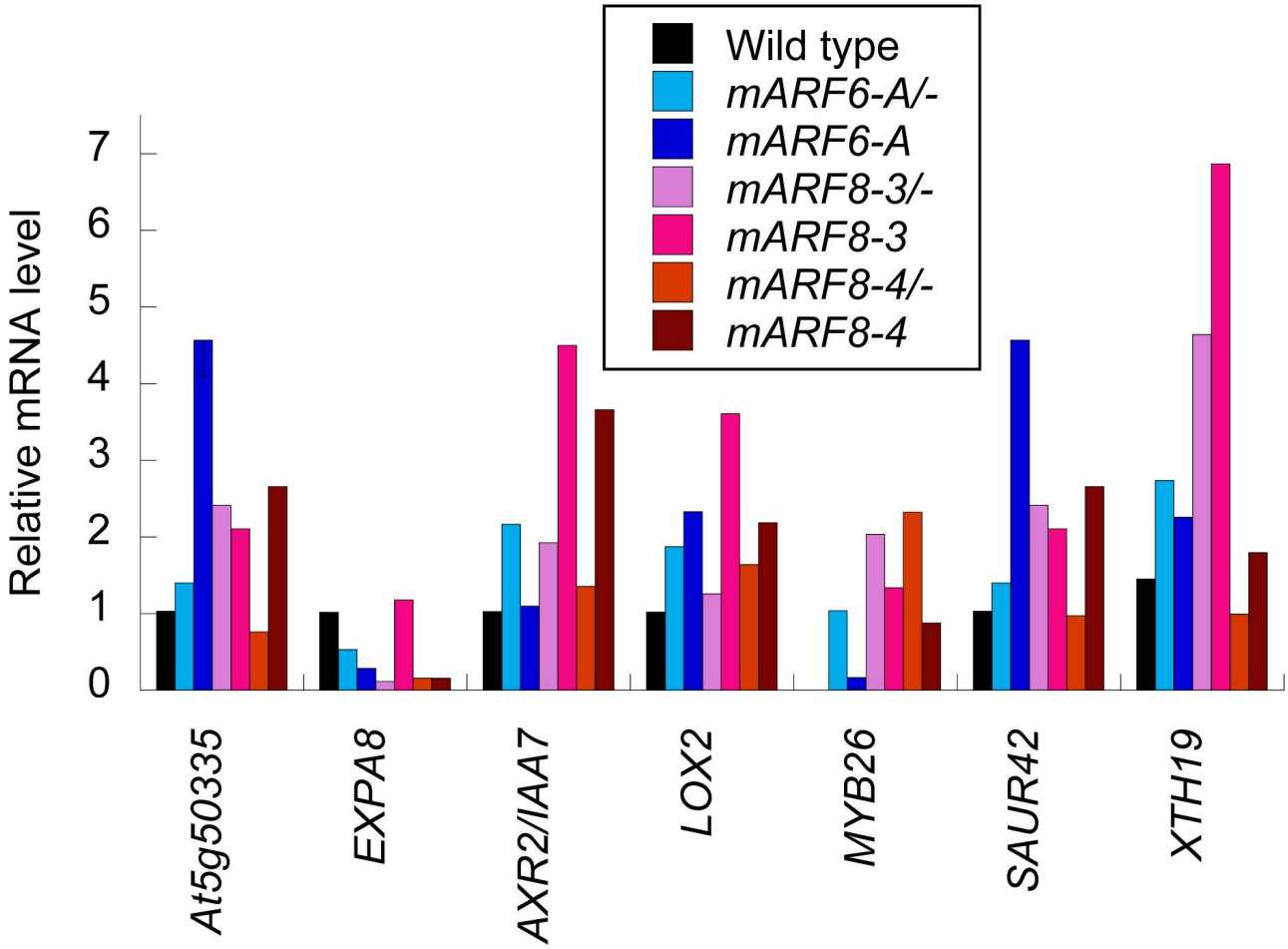

Figure S5. qRT-PCR of mRNA levels in stage 11 *mARF* stamens.

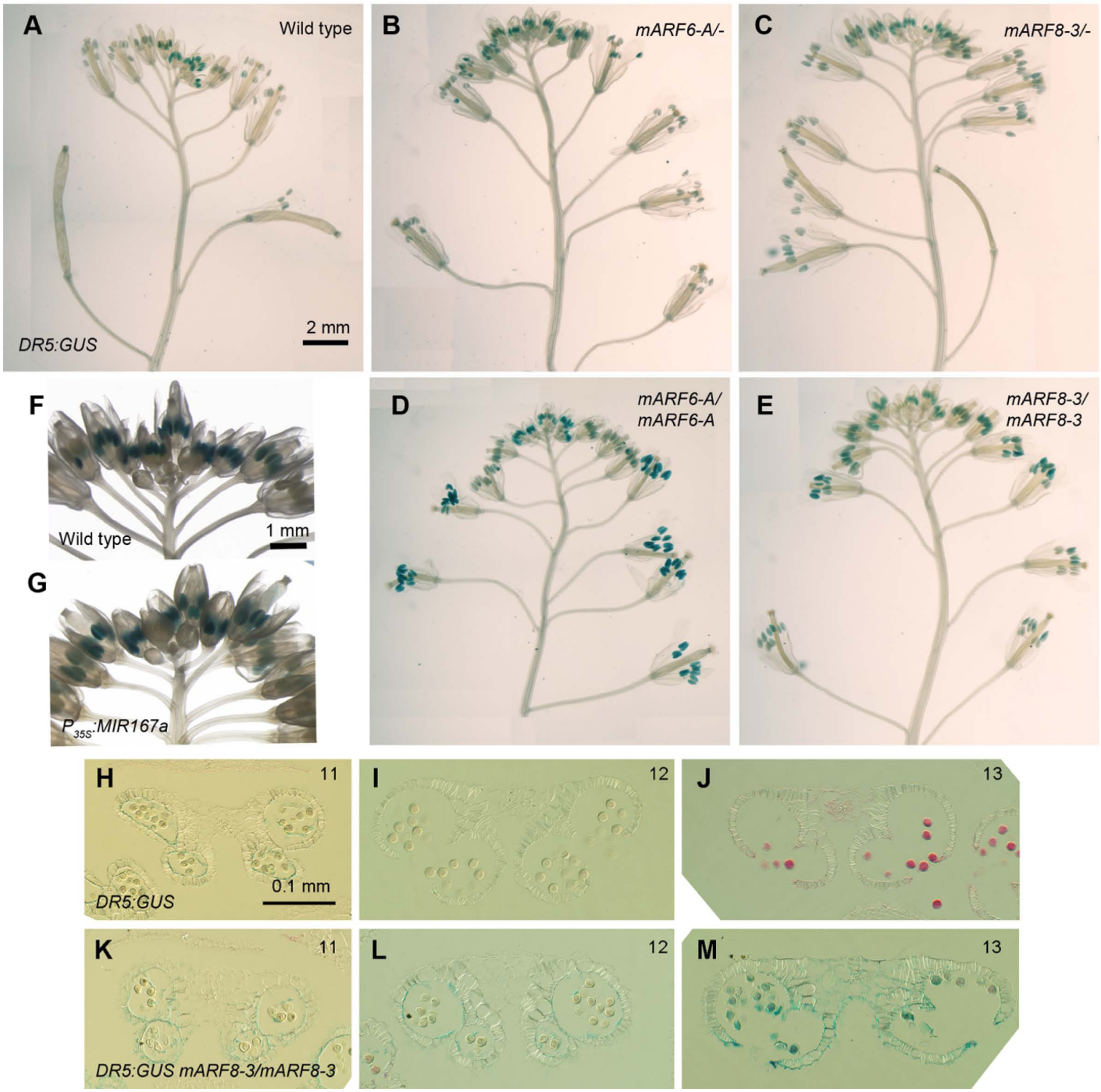

Figure S6. *DR5:GUS* expression in *mARF6*, *mARF8*, and *P35S:MIR167a* flowers and anthers.
A-G) X-Gluc staining of inflorescences carrying the auxin-response reporter DR5:GUS in the indicated genetic backgrounds. Composite images are shown and were obtained by splicing together multiple images from different portions of the specimen. H-J) Sections of X-Gluc-stained *DR5:GUS wild-type* anthers at indicated stages. K-M) Sections of X-Gluc-stained *DR5:GUS mARF8-3* anthers at indicated stages. Brightness of some images was increased for clarity. Scale bars, 2 mm (A-E), 1 mm (F,G), 0.1 mm (H-M).

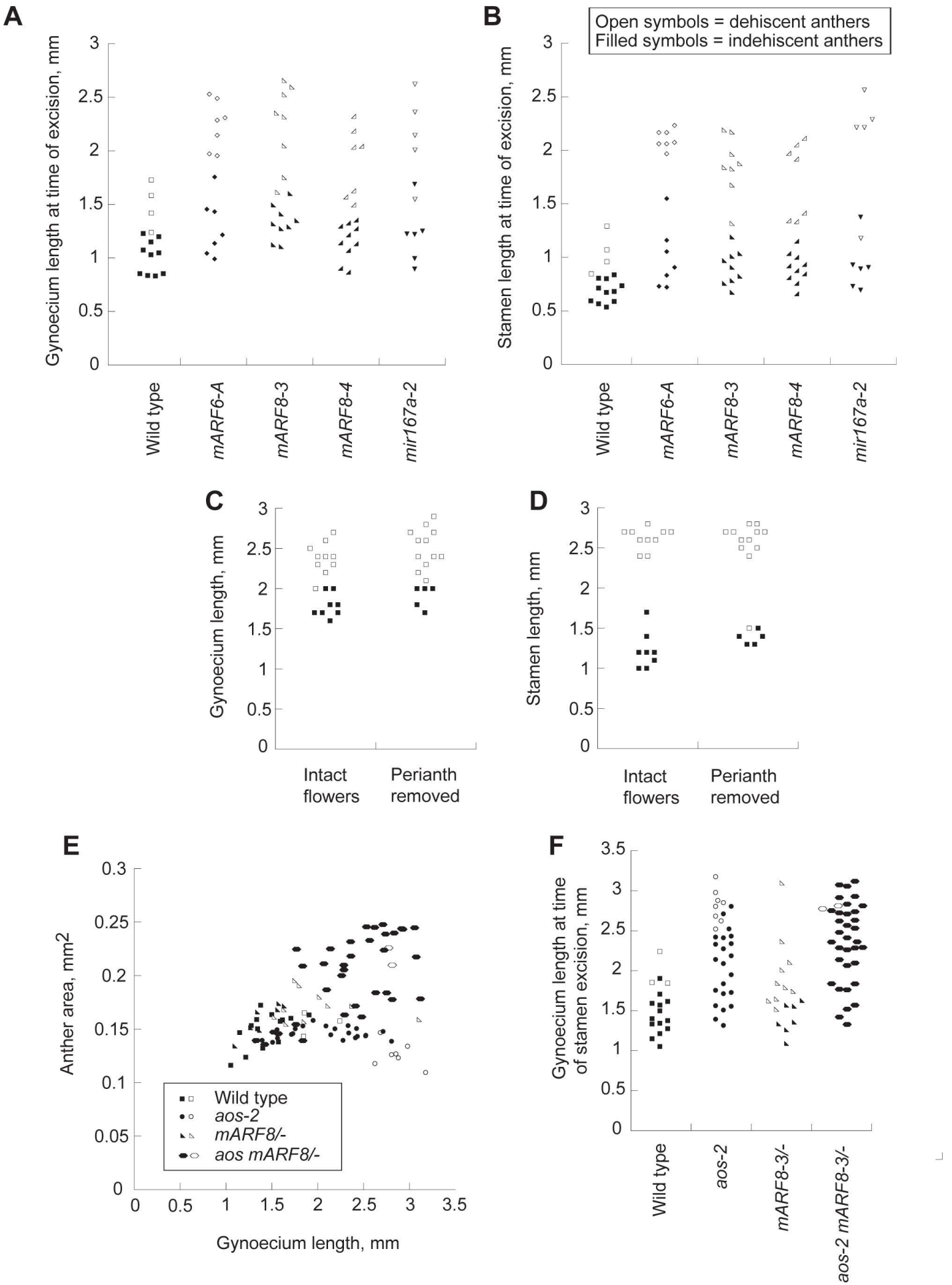

Figure S7. Anther competence to dehisce.

A,B) Gynoecium and stamen lengths at the time of excision from flowers, and subsequent dehiscence, for the indicated genotypes.

C,D) Gynoecium and stamen lengths and anther dehiscence of wild-type stage 11-12 flower buds that were either left intact or whose perianth (sepals and petals) had been removed. Flowers were left on the growing parent plant during the experiment. Gynoecium and stamen lengths were measured and anther dehiscence was assessed 24h after perianth removal.

E,F) Effects of *aos-2* and *mARF8-3/-* genotypes on anther dehiscence. Gynoecium length and anther areas were measured from images taken at the time of stamen excision, and subsequent anther dehiscence assessed.

For all panels, each point represents one flower, and open/closed symbols indicate whether the majority of anthers on that flower subsequently dehisced (open symbols) or not (closed symbols).

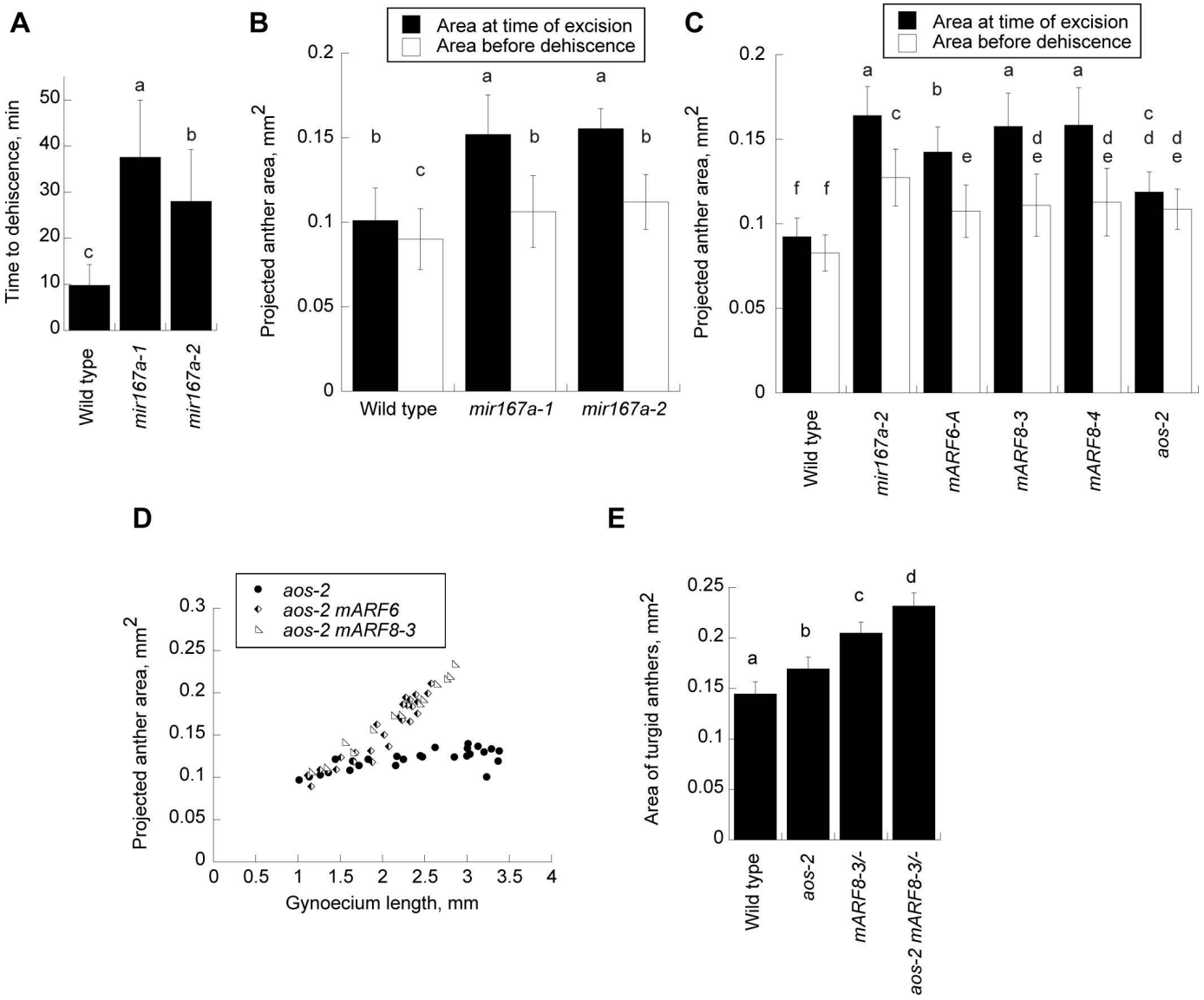

Figure S8. Dehiscence of turgid stage 13 anthers and effects of *aos-2* on anther size.
A-C) Anther dehiscence timing (A) and anther projected area change (B,C) of anthers from excised stamens of stage 13-14 flowers of indicated genotypes. Figure 8M shows dehiscence timing data corresponding to the experiment in panel C.
D) Projected anther areas of indicated genotypes. Gynoecium length was used as a standard indicate flower stage.
E) Projected areas of turgid anthers of indicated genotype
In A-C and E, 2 cm inflorescence apices were inserted in agar in sealed plates for 2d, stamens were then excised and anther dehiscence subsequently monitored over time. Anther areas were measured from the earliest available image after stamen excision and from the last available image before visible dehiscence. Letters indicate statistical classes based on Tukey's Honestly Significant Difference test.

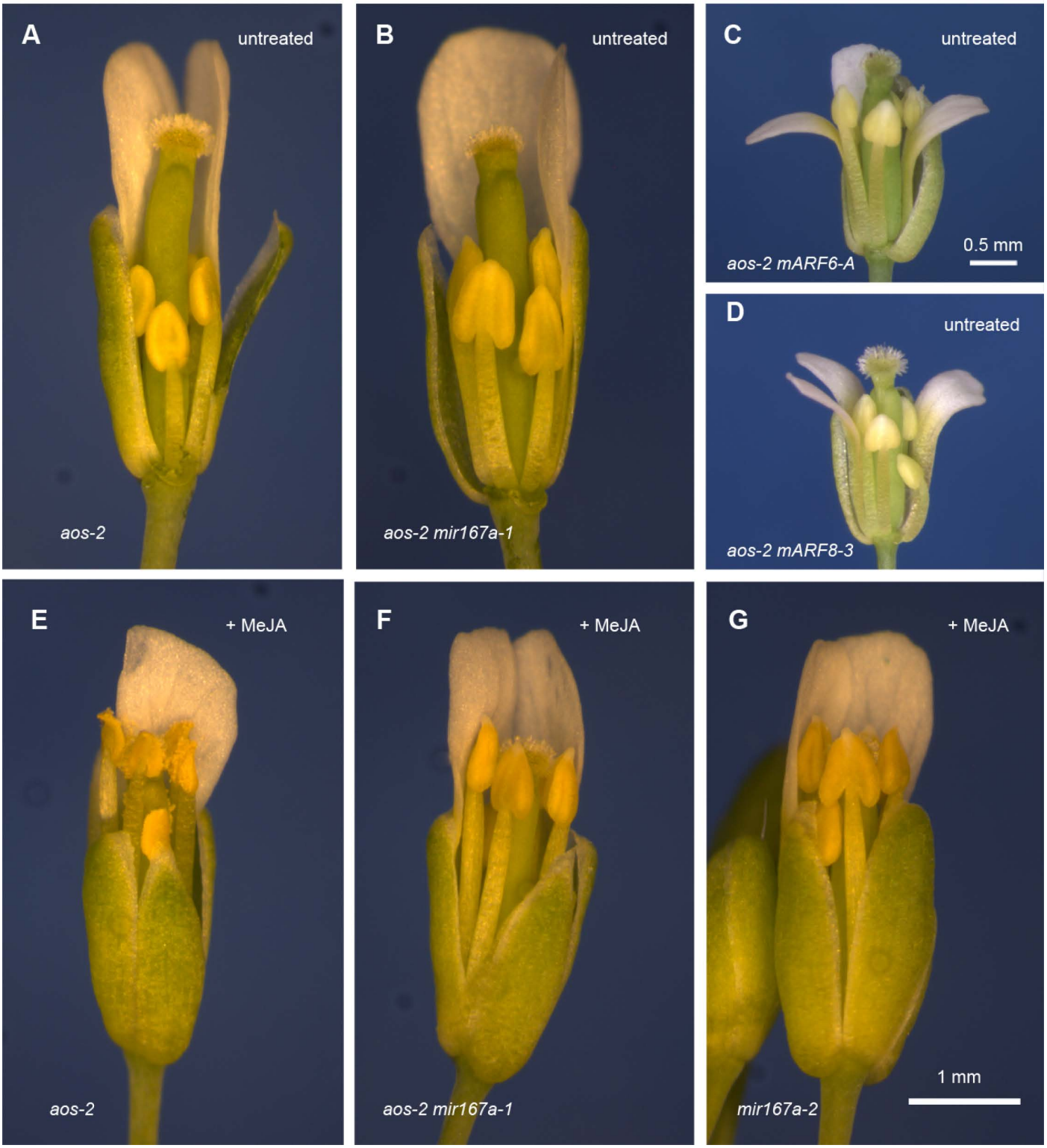

Figure S9. Genetic interactions between *aos-2* and miR167 pathway mutations.
A-D) Stage 13 flowers of indicated genotypes of untreated apices.
E-G) Stage 13 flowers of indicated genotypes from apices that had been treated with methyl jasmonate (MeJA) two days before the flower opened. Some petals and stamens were removed so as to expose the stamens and gynoecium for photography. In A, B, D, E, and F, flowers that had already opened at the time of MeJA treatment were removed. Scale bars: A, B, D, E, and F, 1 mm; C, D, 0.5 mm.

Tables S1 - S11

Click here to download Tables S1 - S11